https://doi.org/10.5194/egusphere-2026-4073
Preprint. Discussion started: 21 July 2026

Improved Method for Merging Particle Filter Using Random Merging Coefficients

Naoki Hiramoto[1], Genta Ueno[1,2], and Daisuke Murakami[1,2]

[1]Statistical Science Program, Graduate Institute for Advanced Studies, SOKENDAI, Tokyo, Japan
[2]The Institute of Statistical Mathematics, Tokyo, Japan

Correspondence: Naoki Hiramoto (hiramoto.naoki@ism.ac.jp)

Abstract.

This paper proposes an improved method for the merging particle filter (MPF), which is employed as a data assimilation technique for nonlinear systems. While MPF achieves good root mean square error (RMSE) with a small number of particles relative to the basic particle filter, it suffers from a lack of systematic guidelines in setting merging coefficients, and estimation accuracy plateaus when the number of particles increases. Here, merging coefficients refer to the weight parameters used in the linear combination of multiple particles, with the constraints that their sum equals 1 and their sum of squares equals 1. However, these coefficients are chosen empirically, without theoretical understanding. In this study, we propose the randomized merging particle filter (RMPF) that randomly generates the merging coefficients and obtains estimates from the pre-merging distribution. Furthermore, a theoretical analysis clarifies how the merging dimension shapes the merged-particle distribution, casting its selection as a bias–variance trade-off that we resolve in practice by likelihood maximization. Numerical experimental results using Lorenz-63 and Lorenz-96 models demonstrated highly accurate estimation by RMPF.

1 Introduction

Data assimilation estimates state variables by combining time-series observations with numerical models and has thus become indispensable in diverse applications, such as meteorological and oceanographic simulations, robotics, and medical applications (Nakano and Higuchi, 2009, 2012; Ito et al., 2024; Gustafsson, 2010; Kummert et al., 2021). Monte Carlo methods based on Bayesian theory are the most common choice for nonlinear and non-Gaussian systems, with the particle filter (PF) (Kitagawa, 1996; Gordon et al., 1993) being a representative example. However, PF suffers from the degeneracy problem and is prone to failure because weight bias progresses rapidly, and in high dimensions, effective sample size is known to decrease exponentially (Snyder et al., 2008). To address this problem, various methods have been proposed; however, these often introduce trade-offs, such as increased computational cost and loss of higher-order moments (Nakano et al., 2007).

Merging particle filter (MPF) redistributes particles by replacing multiple particles with 'merged particles' through a linear combination of several particles, preserving mean and variance. The linear combination is performed using merging coefficients, which are weight parameters that must satisfy specific constraints: their sum and their sum of squares must equal 1. However, there are two problems. First, there is no systematic approach for setting appropriate merging coefficients, and prior

https://doi.org/10.5194/egusphere-2026-4073
Preprint. Discussion started: 21 July 2026

Table 1. Main notation

Symbol	Meaning and dimension
$\mathbf{x}_t \in \mathbb{R}^d$	Internal state vector at time t
$\mathbf{y}_t \in \mathbb{R}^m$	Observation vector (m components)
$F_t(\cdot)$	System model (time update operator)
$H_t(\cdot)$	Observation model (mapping to observation space)
$\mathbf{v}_t$, $\mathbf{w}_t$	System noise, observation noise
N	Number of particles
n	Number of particles for merging ($n \geq 3$)
$\boldsymbol{\alpha} = (\alpha_1, \ldots, \alpha_n)$	Merging coefficients; $\sum \alpha_j = 1$, $\sum \alpha_j^2 = 1$
π	Importance weights
$\tilde{\pi}$	Normalized importance weights
$\hat{\mathbf{x}}_t$	Estimated state (particle mean)
$\boldsymbol{\Sigma}_t$	Estimated covariance matrix

work offers only heuristic, experimental choices (Nakano et al., 2007; Shen et al., 2017). Second, estimation accuracy saturates, with further increases in the number of particles yielding no improvement (Nakano et al., 2007; Shen et al., 2017).

In this study, we propose the randomized merging particle filter (RMPF) to solve these challenges presented by MPF. RMPF solves the problems of MPF by (i) randomly generating merging coefficients from a spherical uniform distribution and (ii) computing estimates from the particle average at the pre-merging step. The remainder of this paper is organized as follows. Section 2 presents the problem setting, background on particle filters, and related work. Section 3 details the RMPF algorithm and its theoretical properties. In Section 4, the probability density of merged particles is analyzed. In Section 5, the effect of the merging dimension on distributional characteristics is analyzed. Sections 6 and 7 report numerical experiments on the Lorenz63 and Lorenz96 models, respectively. In Section 8, practical guidelines are proposed for selecting the merging dimension via likelihood maximization. Section 9 provides a discussion. Section 10 presents the conclusions and future directions. Table 1 summarizes the main notation used throughout this paper.

2 Related Work and Background

Particle filters represent a general framework for nonlinear data assimilation, as they make no assumptions about the form of the posterior distribution and can handle nonlinearities and non-Gaussian noise. By representing the posterior distribution through a set of weighted samples (particles), particle filters can capture complex multimodal distributions and provide consistent estimates even in highly nonlinear scenarios. This flexibility makes particle filters particularly attractive in challenging applications although PFs face their own computational and theoretical challenges, particularly in high-dimensional systems.

https://doi.org/10.5194/egusphere-2026-4073
Preprint. Discussion started: 21 July 2026

Algorithm 1 Particle Filter (PF)

Generate initial ensemble $\{\mathbf{x}_0^i\}_{i=1}^N$
for $t = 1$ to T **do**
  for $i = 1$ to N **do**
    Generate system noise $\mathbf{v}_t^i$ {Prediction step}
    Compute $\mathbf{x}_t^i = F_t(\mathbf{x}_{t-1}^i, \mathbf{v}_t^i)$
  end for
  for $i = 1$ to N **do**
    Compute likelihood $\pi_t^i = p(\mathbf{y}_t|\mathbf{x}_t^i)$ {Filtering step}
  end for
  Normalize weights: $\tilde{\pi}_t^i = \frac{\pi_t^i}{\sum_{j=1}^N \pi_t^j}$
  Resample N particles from $\{\mathbf{x}_t^i\}_{i=1}^N$ based on normalized weights $\{\tilde{\pi}_t^i\}$ {Resampling}
end for

2.1 Particle Filter for State Space Models

Building upon the general data assimilation framework, we now formalize the particle filter approach for state space models. The state space model at time step t is formulated as follows:

$$\mathbf{x}_t = F_t(\mathbf{x}_{t-1}, \mathbf{v}_t), \tag{1}$$

$$\mathbf{y}_t = H_t(\mathbf{x}_t, \mathbf{w}_t), \tag{2}$$

where $\mathbf{x}_t$ is the internal state vector; $\mathbf{y}_t$ is the observation vector; and $\mathbf{y}_{1:t}$ represents the sequence of observation vectors $(\mathbf{y}_1, \mathbf{y}_2, \ldots, \mathbf{y}_t)$. Additionally, $\mathbf{v}_t$ and $\mathbf{w}_t$ represent system noise and observation noise, respectively. F_t and H_t denote the system and observation models, respectively.

The PF is a method that approximates the posterior distribution $p(\mathbf{x}_t \mid \mathbf{y}_{1:t})$ using an ensemble $\{\mathbf{x}_t^i\}_{i=1}^N$ and weights $\{\pi_t^i\}_{i=1}^N$. The standard algorithm is summarized as follows.

While PF is a highly versatile method applicable to nonlinear and non-Gaussian systems, several important practical challenges exist. The most serious problem is weight degeneracy. Over time, only a few particles acquire very large weights, and the weights of other particles become nearly zero (Snyder et al., 2008; Li et al., 2014; Daum and Huang, 2011; Bengtsson et al., 2008). This phenomenon is characterized by what Snyder et al. (2008) describe as a "collapse" such that "with high probability a single member is assigned a posterior weight close to one while all other members have vanishingly small weights" (Snyder et al., 2008). This degeneracy is also referred to as "impoverishment" or "sample attrition," resulting in the loss of particle diversity and significant deterioration in the approximation accuracy of the posterior distribution. This is fundamentally caused by the curse of dimensionality: as the dimension d of the state space increases, the required number of particles N grows exponentially (Bengtsson et al., 2008; Snyder et al., 2008; Slivinski and Snyder, 2016), making particle filters computationally

https://doi.org/10.5194/egusphere-2026-4073
Preprint. Discussion started: 21 July 2026

intractable in high-dimensional systems such as those encountered in atmospheric data assimilation (Bengtsson et al., 2008; Slivinski and Snyder, 2016).

To address these degeneracy issues, several improvement methods have been proposed, including auxiliary particle filters that use superior proposal distributions (Pitt and Shephard, 1999), localized particle filters that reduce dimensionality by localizing observation domains (Poterjoy, 2016), proposal density methods that guide particles toward future observations (Van Leeuwen, 2010), and ensemble-based methods that combine particle filtering with (ensemble) Kalman filter techniques (Hoteit et al., 2012; Van Leeuwen et al., 2019). While these methods are effective in specific contexts, they often introduce trade-offs between computational efficiency, theoretical rigor, and practical implementation complexity.

Among these approaches, regularized particle filter methods have received attention for their ability to maintain particle diversity through regularization techniques. The seminal work by Musso et al. (2001) and Liu and West (2001) introduced kernel-based regularization methods that smooth the empirical particle distribution using kernel density estimation (Musso et al., 2001; Liu and West, 2001). Their approach replaces the discrete particle representation with a continuous approximation by convolving particles with Gaussian kernels, effectively creating a mixture of Gaussians that preserves the first and second moments while enhancing particle diversity. Chen and Haykin (2002) provided theoretical foundations for regularization theory in the context of particle filtering (Chen and Haykin, 2002). Oudjane in 2000 and Rossi in 2004 further developed kernel approximation techniques in parameter-augmented state spaces (Oudjane, 2000; Rossi, 2004). However, these kernel-based methods require careful selection of bandwidth parameters to minimize the mean integrated square error between the true conditional density and regularized empirical density, whereby the computational overhead of kernel density estimation becomes prohibitive in high-dimensional systems.

As an alternative approach for addressing the degeneracy problem, the MPF proposed by Nakano et al. (2007) has attracted attention as a method that effectively mitigates the degeneracy problem (Van Leeuwen et al., 2019; Vetra-Carvalho et al., 2018; Maclean et al., 2017; Maclean and Spiller, 2020; Cooper and Perez, 2018). MPF was proposed to reduce the degeneracy and computational load in PF. MPF subsamples a subset of particles from the prediction step and generates new particles by merging them with weighted sums as follows:

The key difference from the standard PF is the addition of lines 12-15, which constitute the merging operation. Instead of directly using resampled particles, MPF performs extended resampling (line 12) to obtain $N \times n$ particles, then merges them using linear combinations (lines 13-15) to generate N new particles for the next time step.

In the merging operation, the merging coefficients $\boldsymbol{\alpha} = (\alpha_1, \alpha_2, \ldots, \alpha_n)$ are set to satisfy the constraints

$$\sum_{j=1}^{n} \alpha_j = 1 \quad \text{and} \quad \sum_{j=1}^{n} \alpha_j^2 = 1. \tag{3}$$

These constraints preserve the first and second moments of the original particle distribution while enabling improved particle diversity and preventing degeneracy. Numerical experiments showed significant root mean square error (RMSE) improvements compared to standard PF, particularly with a small number of particles (Nakano et al., 2007).

Despite these advantages, MPF faces several challenges, as identified by Nakano et al. (2007), considering both experimental and theoretical perspectives. The first challenge is the lack of an established method for setting the merging coefficients

https://doi.org/10.5194/egusphere-2026-4073
Preprint. Discussion started: 21 July 2026

Algorithm 2 Merging Particle Filter (MPF)

Generate initial ensemble $\{\mathbf{x}_0^i\}_{i=1}^N$
Set $n \geq 3$ for the number of particles to merge and coefficients $\{\alpha_j\}_{j=1}^n$
for $t = 1$ to T **do**
  for $i = 1$ to N **do**
    Generate system noise $\mathbf{v}_t^i$ {Prediction step}
    Compute $\mathbf{x}_t^i = F_t(\mathbf{x}_{t-1}^i, \mathbf{v}_t^i)$
  end for
  for $i = 1$ to N **do**
    Compute likelihood $\pi_t^i = p(\mathbf{y}_t|\mathbf{x}_t^i)$ {Filtering step}
  end for
  Normalize weights: $\tilde{\pi}_t^i = \frac{\pi_t^i}{\sum_{j=1}^N \pi_t^j}$
  Resample $N \times n$ particles $\{\hat{\mathbf{x}}_t^{j,i}\}$ from $\{\mathbf{x}_t^i\}_{i=1}^N$ based on normalized weights $\{\tilde{\pi}_t^i\}_{i=1}^N$ {Extended resampling}
  for $i = 1$ to N **do**
    $\mathbf{x}_t^i = \sum_{j=1}^n \alpha_j \hat{\mathbf{x}}_t^{j,i}$ {Merging step}
  end for
  Compute post-merging estimate: $\hat{\mathbf{x}}_t = \frac{1}{N}\sum_{i=1}^N \mathbf{x}_t^i$
end for

$\boldsymbol{\alpha}$. The merging operation requires selecting particle weights (merging coefficients) that satisfy Eq. (3). For $n \geq 3$, there exist infinitely many $\boldsymbol{\alpha}$ satisfying these constraints; however, it is unclear which coefficients are most effective for estimation accuracy. Nakano et al. (2007) presented specific examples such as $\alpha_1 = \frac{3}{4}, \alpha_2 = \frac{\sqrt{13}+1}{8}, \alpha_3 = -\frac{\sqrt{13}-1}{8}$, but these were verified on limited numerical examples. There are no optimal selection guidelines, and a systematic understanding of how merging coefficients affect estimation performance has not been established. The second challenge is RMSE saturation with increasing particle numbers. Although increasing the number of particles N in PF improves accuracy, MPF exhibits a "saturation phenomenon" such that RMSE stops improving beyond a certain value, eventually making standard PF perform better (Nakano et al., 2007). This is presumed to occur because the merging operations in MPF simplify the shape of particle distributions, preventing the full utilization of abundant particles (Nakano et al., 2007).

To address these challenges, this study proposes the RMPF described in the next section. RMPF introduces random merging coefficients and estimates from pre-merging distributions to address the problems of MPF while inheriting its advantages.

https://doi.org/10.5194/egusphere-2026-4073
Preprint. Discussion started: 21 July 2026

3 Proposed Method: Randomized Merging Particle Filter (RMPF)

3.1 Overview

The RMPF has two key features that solve the limitations of the conventional MPF. First, RMPF employs random merging coefficient generation, whereby coefficients $\boldsymbol{\alpha}$ are randomly generated to satisfy the constraints in Eq. 3, using a different $\boldsymbol{\alpha}$ for each merging operation. This randomization eliminates the reliance on empirical coefficient selection and enhances particle diversity. Second, RMPF adopts pre-merging distribution estimates. Rather than using the mean of post-merging particles as in the conventional MPF, the mean of the pre-merging particle distribution (at pre-merging step) is used as the estimate. The merging operation serves as an auxiliary process in suppressing particle degeneracy while preserving the distributional information obtained from observations.

3.2 RMPF Algorithm

The overall algorithm of RMPF proposed in this study is detailed in Algorithm 3. Here, we denote the number of particles by N, merging size by n, and system and observation models at time t by F_t and H_t, respectively. The detailed generation method for merging coefficients $\boldsymbol{\alpha}^{(i)}$, which represent the coefficients used in the i-th merging operation, is explained in the subsequent Section 3.3.

The key feature of this algorithm is the random generation of merging coefficients. Unlike the conventional MPF that uses fixed merging coefficients, RMPF generates different random merging coefficients for each particle. This approach enhances distributional diversity and enables more flexible particle representation. Additionally, by using the weighted mean $\hat{\mathbf{x}}_t$ obtained during pre-merging step as the estimate at time t, the merging operation in MPF is treated as an auxiliary for the next time step, whereby state estimation is performed based on the pre-merging particle ensemble with less information loss. In numerical experiments, this significantly alleviated the accuracy saturation with increasing number of particles previously pointed out in MPF.

For computational efficiency in practical implementations, the merging coefficients $\{\alpha_j^i\}_{j=1}^n$ can be pre-generated and reused across multiple time steps or particles, thereby significantly reducing the computational overhead while maintaining the theoretical benefits of randomization. This approach provides a practical trade-off between theoretical rigor and computational efficiency.

3.3 Addressing Challenge 1: Method for Generating Merging Coefficients

When generating merging coefficients $\boldsymbol{\alpha} = (\alpha_1, \ldots, \alpha_n)$, the following constraints must be satisfied:

$$\sum_{j=1}^{n} \alpha_j = 1, \quad \sum_{j=1}^{n} \alpha_j^2 = 1. \tag{4}$$

To generate merging coefficients that satisfy these constraints, we developed a method inspired by the spherical uniform sampling approach of Muller (1959) (Muller, 1959). The algorithm first samples an n-dimensional vector $\mathbf{u} = (u_1, \ldots, u_n)$

https://doi.org/10.5194/egusphere-2026-4073
Preprint. Discussion started: 21 July 2026

Algorithm 3 Randomized Merging Particle Filter (RMPF)

Generate initial ensemble $\{\mathbf{x}_0^i\}_{i=1}^N$
Set $n \geq 3$ as the number of particles to merge
for $t = 1$ to T **do**
  for $i = 1$ to N **do**
    Generate system noise $\mathbf{v}_t^i$ {Prediction step}
    Compute $\mathbf{x}_t^i = F_t(\mathbf{x}_{t-1}^i, \mathbf{v}_t^i)$
  end for
  for $i = 1$ to N **do**
    Compute likelihood $\pi_t^i = p(\mathbf{y}_t|\mathbf{x}_t^i)$ {Filtering step}
  end for
  Normalize weights: $\tilde{\pi}_t^i = \frac{\pi_t^i}{\sum_{j=1}^N \pi_t^j}$
  Resample $N \times n$ particles $\{\hat{\mathbf{x}}_t^{j,i}\}$ from $\{\mathbf{x}_t^i\}_{i=1}^N$ based on normalized weights $\{\tilde{\pi}_t^i\}$ {Extended resampling}
  Compute pre-merging estimate: $\hat{\mathbf{x}}_t = \sum_{i=1}^N \tilde{\pi}_t^i \mathbf{x}_t^i$
  for $i = 1$ to N **do**
    Randomly generate merging coefficients $\{\alpha_j^i\}_{j=1}^n$ {Random coefficient generation and merging}
    $\mathbf{x}_t^i = \sum_{j=1}^n \alpha_j^i \hat{\mathbf{x}}_t^{j,i}$
  end for
  State estimate: Adopt $\hat{\mathbf{x}}_t$
end for

from the standard normal distribution. To ensure the sum constraint, we subtract the mean: $\mathbf{z} = \mathbf{u} - \bar{u}\mathbf{1}_n$ where $\bar{u} = \frac{1}{n}\sum_{j=1}^n u_j$ and $\mathbf{1}_n$ is an n-dimensional vector of ones. The vector $\mathbf{z}$ is then normalized to the unit sphere: $\mathbf{v} = \mathbf{z}/\|\mathbf{z}\|$. Finally, scaling and translation are applied to $\boldsymbol{\alpha} = \mathbf{v}\sqrt{\frac{n-1}{n}} + \frac{1}{n}\mathbf{1}_n$, to satisfy both constraints:

We verified that the merging coefficients $\boldsymbol{\alpha}$ generated by this algorithm satisfy the constraint conditions. First, regarding the sum, since $\mathbf{v}$ is a vector on the unit sphere with $\mathbf{v} \cdot \mathbf{1}_n = 0$ (sum of elements is 0):

$$\begin{aligned}\sum_{j=1}^n \alpha_j &= \sum_{j=1}^n \left(v_j \sqrt{\frac{n-1}{n}} + \frac{1}{n} \right) \\ &= \sqrt{\frac{n-1}{n}} \sum_{j=1}^n v_j + \frac{n}{n} = 0 + 1 = 1 \end{aligned} \tag{5}$$

Next, regarding the sum of squares, as $\mathbf{v}$ is a unit vector ($\|\mathbf{v}\|^2 = 1$):

$$\begin{aligned}\|\boldsymbol{\alpha}\|^2 &= \left\| \sqrt{\frac{n-1}{n}}\mathbf{v} + \frac{1}{n}\mathbf{1}_n \right\|^2 = \frac{n-1}{n}\|\mathbf{v}\|^2 + \frac{1}{n^2}\|\mathbf{1}_n\|^2 \\ &= \frac{n-1}{n} + \frac{n}{n^2} = \frac{n-1}{n} + \frac{1}{n} = 1. \end{aligned} \tag{6}$$

https://doi.org/10.5194/egusphere-2026-4073
Preprint. Discussion started: 21 July 2026

Here, the cross term vanishes because $\mathbf{v}$ and $\mathbf{1}_n$ are orthogonal. The preservation of the first and second moments when using random merging coefficients can be demonstrated using methods similar to those of Nakano et al. (2007); the detailed proofs are provided in the Appendix.

3.4 Addressing Challenge 2: Utilization of Pre-merging Distribution

In MPF, the post-merging particle ensemble is typically treated as the "filter distribution," and its weighted mean is used as the estimate. However, the merging operation may cause unimodalization of the distribution shape or information loss, including the loss of higher-order moments (Nakano et al., 2007; Vetra-Carvalho et al., 2018). In the RMPF proposed in this study, the mean of the particle ensemble immediately after weight calculation is adopted as the estimate based on pre-merging observations.

$$\hat{\mathbf{x}}_t = \sum_{i=1}^{N} \tilde{\pi}_t^i \mathbf{x}_t^i \tag{7}$$

This approach is motivated by two key considerations: first, the likelihood weights $\{\pi_t^i\}_{i=1}^N$ are computed at the pre-merging step at time t and cannot be utilized at the post-merging step; second, the influence on estimation accuracy of the distribution shape modified by the merging operation is avoided. By computing the estimate using pre-merging likelihoods, the merging operation is treated as a process for enhancing particle exploration in subsequent time steps, performing state estimation at the timing most faithful to the filter distribution—immediately after resampling—to preserve the original observational information. This enables estimation while preserving distributions containing multiple modes as much as possible, which alleviates the problem of accuracy saturation.

4 Theoretical Analysis: Probability Density of Merged Particles

In this section, we derive the probability density $p(\mathbf{x}_{\text{merged}} \mid X)$ of merged particles $\mathbf{x}_{\text{merged}} \in \mathbb{R}^d$ using the merging particle matrix $X = [\mathbf{x}^1, \ldots, \mathbf{x}^n] \in \mathbb{R}^{d \times n}$. Here, d represents the dimension of the state vector to be estimated, where each particle $\mathbf{x}^i$ is a d-dimensional vector. The parameter n denotes the number of particles to be merged.

4.1 Mathematical Framework

The merging coefficients $\boldsymbol{\alpha} = (\alpha_1, \ldots, \alpha_n)^T$ satisfy

$$\sum_{j=1}^{n} \alpha_j = 1, \qquad \sum_{j=1}^{n} \alpha_j^2 = 1 \tag{8}$$

and the merged particles are given by

$$\mathbf{x}_{\text{merged}} = X\boldsymbol{\alpha}. \tag{9}$$

https://doi.org/10.5194/egusphere-2026-4073
Preprint. Discussion started: 21 July 2026

To consolidate constraints (8)–(9), we define an augmented matrix

$$A = \begin{bmatrix} \mathbf{1}_n^T \\ X \end{bmatrix} \in \mathbb{R}^{(d+1)\times n} \tag{10}$$

and consider a $d+1$-dimensional linear system:

$$A\boldsymbol{\alpha} = \begin{bmatrix} 1 \\ \mathbf{x}_{\text{merged}} \end{bmatrix}. \tag{11}$$

The analysis of the solution space depends critically on the relationship between the number of particles to merge, n, and state dimension d.

4.2 Case 1: Ellipsoid Embedding ($n \leq d+1$)

When $n \leq d+1$ and X has full column rank, $\text{rank}(A) = n$, which implies $\ker(A) = \{0\}$. In this case, the mapping $\boldsymbol{\alpha} \mapsto \mathbf{x}_{\text{merged}} = X\boldsymbol{\alpha}$ is injective, meaning that each merged particle $\mathbf{x}_{\text{merged}}$ corresponds to a unique merging coefficient vector $\boldsymbol{\alpha}$.

Decomposing $\boldsymbol{\alpha}$ as

$$\boldsymbol{\alpha} = \boldsymbol{\mu} + \mathbf{v}, \quad \boldsymbol{\mu} := \tfrac{1}{n}\mathbf{1}_n \ , \quad \mathbf{1}_n^\top \mathbf{v} = 0, \tag{12}$$

and defining $\bar{\mathbf{x}} := X\boldsymbol{\mu}$, the constraint $A\boldsymbol{\alpha} = \begin{bmatrix} 1 \\ \mathbf{x}_{\text{merged}} \end{bmatrix}$ reduces to

$$X\,\mathbf{v} = \mathbf{x}_{\text{merged}} - \bar{\mathbf{x}}. \tag{13}$$

Choosing the minimum–norm solution yields

$$\mathbf{v} = X^+\big(\mathbf{x}_{\text{merged}} - \bar{\mathbf{x}}\big). \tag{14}$$

where X^+ is the left pseudoinverse of X. From the norm constraint $\|\boldsymbol{\alpha}\|^2 = 1$ and using orthogonality

$$\|\boldsymbol{\alpha}\|^2 = \|\boldsymbol{\mu}\|^2 + \|\mathbf{v}\|^2, \qquad \boldsymbol{\mu}^\top \mathbf{v} = 0. \tag{15}$$

This yields an ellipsoid equation:

$$\frac{n-1}{n} = (\mathbf{x}_{\text{merged}} - \bar{\mathbf{x}})^\top (XX^\top)^+ (\mathbf{x}_{\text{merged}} - \bar{\mathbf{x}}). \tag{16}$$

The right hand side of this equation represents the squared generalized Mahalanobis distance from particle mean $\bar{\mathbf{x}}$ to merged particle $\mathbf{x}_{\text{merged}}$. The feasible set of merged particles forms an $(n-1)$-dimensional ellipsoid surface with the specified Mahalanobis distance.

https://doi.org/10.5194/egusphere-2026-4073
Preprint. Discussion started: 21 July 2026

4.3 Case 2: Ball Projection ($n > d+1$)

4.3.1 Probability density and normalization for a fixed particle set

Let $r = \mathrm{rank}(A) \le d+1$ and set $m = n - r \ge 0$. The minimum–norm particular solution and null–space parameterization are expressed as

$$\boldsymbol{\alpha}^* \;=\; A^{+}\begin{bmatrix} 1 \\ \mathbf{x}_{\mathrm{merged}} \end{bmatrix}, \qquad \boldsymbol{\alpha} \;=\; \boldsymbol{\alpha}^* + B\boldsymbol{z},\;\; \boldsymbol{z}\in\mathbb{R}^m, \tag{17}$$

where the columns of $B \in \mathbb{R}^{n\times m}$ form an orthonormal basis of $\ker(A)$. Let $P = I_n - \frac{1}{n}\mathbf{1}_n\mathbf{1}_n^\top$ and note that

$$\|\boldsymbol{\alpha}^*\|^2 \;=\; \frac{1}{n} + (\mathbf{x}_{\mathrm{merged}} - \bar{\mathbf{x}})^\top (XPX^\top)^{+} (\mathbf{x}_{\mathrm{merged}} - \bar{\mathbf{x}}). \tag{18}$$

Using $\boldsymbol{\alpha}^* \perp B\boldsymbol{z}$ and the constraint $\|\boldsymbol{\alpha}\|^2 = 1$, we define

$$\begin{aligned} R^2(\mathbf{x}_{\mathrm{merged}}) := \frac{n-1}{n} \\ - (\mathbf{x}_{\mathrm{merged}} - \bar{\mathbf{x}})^\top (XPX^\top)^{+} (\mathbf{x}_{\mathrm{merged}} - \bar{\mathbf{x}}). \end{aligned} \tag{19}$$

Then

$$\|\boldsymbol{z}\|^2 \;=\; R^2(\mathbf{x}_{\mathrm{merged}}). \tag{20}$$

By definition, feasibility requires $R^2(\mathbf{x}_{\mathrm{merged}}) \ge 0$. Hence points with $R^2(\mathbf{x}_{\mathrm{merged}}) < 0$ lie outside the feasibility ellipsoid and have zero probability under the merging operation.

When $R(\mathbf{x}_{\mathrm{merged}}) > 0$, the feasible $\boldsymbol{z}$ lie on sphere $S^{m-1}\big(R(\mathbf{x}_{\mathrm{merged}})\big)$; when $R(\mathbf{x}_{\mathrm{merged}}) = 0$, and the null space collapses to a point. The induced (unnormalized) density in $\mathbf{x}_{\mathrm{merged}}$ is therefore proportional to the volumetric factor—the surface measure of $S^{m-1}(R)$—which scales as R^{m-1}, equivalently to

$$\begin{aligned} p\big(\mathbf{x}_{\mathrm{merged}} \mid X\big) \;\propto\; \big[R^2(\mathbf{x}_{\mathrm{merged}})\big]_+^{\frac{m-2}{2}}, \\ \text{where } [u]_+ := \max\{u, 0\}. \end{aligned} \tag{21}$$

From this geometric view, when $n > d+1$, this case is referred to as volumetric resampling.

To normalize, let $\Sigma = XPX^\top$ have rank $k = r-1$ and choose L so that $\Sigma^+ = L^\top L$. With the change of variables $\xi = L(\mathbf{x}_{\mathrm{merged}} - \bar{\mathbf{x}})$, we have

$$\begin{aligned} (\mathbf{x}_{\mathrm{merged}} - \bar{\mathbf{x}})^\top \Sigma^{+} (\mathbf{x}_{\mathrm{merged}} - \bar{\mathbf{x}}) = \|\xi\|^2, \\ d\mathbf{x}_{\mathrm{merged}} = |\det{}'(\Sigma)|^{-1/2}\, d\xi, \end{aligned} \tag{22}$$

where $\det{}'$ is the product of the nonzero eigenvalues of Σ. Setting $a = \frac{n-1}{n}$ and $\beta = \frac{n-r-2}{2} > -1$, the normalization integral takes the standard unit–ball form

$$\int_{\|\xi\| \le \sqrt{a}} (a - \|\xi\|^2)^{\beta}\, d\xi \;=\; a^{\beta + k/2}\, \frac{\pi^{k/2}\Gamma(\beta+1)}{\Gamma(\beta+1+k/2)}. \tag{23}$$

https://doi.org/10.5194/egusphere-2026-4073
Preprint. Discussion started: 21 July 2026

Therefore, for $\beta > -1$ (equivalently $n > r+1$), the normalized density is

$$p(\mathbf{x}_{\text{merged}} \mid X) = C_{n,r} \, |\det{}'(\Sigma)|^{-1/2} \left[R^2(\mathbf{x}_{\text{merged}})\right]_+^{\frac{n-r-2}{2}}, \qquad \Sigma = XPX^\top, \tag{24}$$

with

$$C_{n,r} = \frac{\Gamma\left(\frac{n-1}{2}\right)}{\pi^{\frac{r-1}{2}}\Gamma\left(\frac{n-r}{2}\right)} \left(\frac{n}{n-1}\right)^{\frac{n-3}{2}}. \tag{25}$$

In the full–rank case $r = d+1$, this simplifies to

$$C_{n,d+1} = \frac{\Gamma\left(\frac{n-1}{2}\right)}{\pi^{\frac{d}{2}}\Gamma\left(\frac{n-d-1}{2}\right)} \left(\frac{n}{n-1}\right)^{\frac{n-3}{2}}. \tag{26}$$

The derivation requires $\beta > -1$, i.e., $n > r+1$. If $n = r+1$ we have $\beta = -\frac{1}{2}$: the density remains integrable but sharply peaks near the boundary. The detailed derivation of the normalization constant is provided in the Appendix.

4.3.2 Application to Particle Filtering: Overall Merged Distribution

After the one-step ahead prediction, before resampling $N \times n$ particles for merging, the normalized weights $\boldsymbol{\pi} = (\tilde{\pi}_1, \ldots, \tilde{\pi}_N)$ are computed in a resampling step. The distribution of the merged particles $\mathbf{x}_{\text{merged}}$ becomes an average of the distribution $p(\mathbf{x}_{\text{merged}} \mid X)$ generated from a specific particle set X over all particle sets sampled according to $\boldsymbol{\pi}$. For an index tuple $I = (i_1, \ldots, i_n)$, define

$$X_I := \left[\mathbf{x}^{(i_1)} \cdots \mathbf{x}^{(i_n)}\right], \qquad P(I \mid \tilde{\boldsymbol{\pi}}) := \prod_{j=1}^{n} \tilde{\pi}_{i_j}. \tag{27}$$

Then the overall mixture is

$$p(\mathbf{x}_{\text{merged}} \mid \tilde{\boldsymbol{\pi}}) = \sum_{I \in [N]^n} P(I \mid \tilde{\boldsymbol{\pi}}) \, p(\mathbf{x}_{\text{merged}} \mid X_I). \tag{28}$$

This framework is common regardless of the relationship between n and d; however, note that the properties of the component $p(\mathbf{x}_{\text{merged}} \mid X)$ differ fundamentally between the cases of $n > d+1$ and $n \leq d+1$.

In the case of $n > d+1$ (volumetric resampling), $p(\mathbf{x}_{\text{merged}} \mid X)$ becomes a probability density function that takes values in a bounded region (a region obtained by projecting a hypersphere) within the d-dimensional space, as given by Eq. (24). Therefore, the overall distribution $p(\mathbf{x}_{\text{merged}} \mid \tilde{\boldsymbol{\pi}})$ becomes a weighted mixture of these probability density functions, forming a continuous and smooth distribution within the state space. This means that the probability density is redistributed among intermediate regions where particles did not originally exist, thereby functioning as a powerful regularization against sample degeneracy.

In the case of $n \leq d+1$ (surface-based resampling), the merged particles $\mathbf{x}_{\text{merged}}$ are restricted to $(n-1)$-dimensional ellipsoidal surfaces, and by continuously sampling coefficients on that surface, the method fills the gaps in the state space

https://doi.org/10.5194/egusphere-2026-4073
Preprint. Discussion started: 21 July 2026

Table 2. Distribution characteristics of RMPF (for $r = d + 1$). The table compares MPF and RMPF as n varies.

Case	Condition	Power Exponent	Distribution Type
Surface-based	$n \leq d+1$	N/A	Ellipsoid surface distribution
Edge concentration	$n = d+2$	$\frac{n-d-3}{2} < 0$	Peripheral concentration
Uniform distribution	$n = d+3$	$\frac{n-d-3}{2} = 0$	Uniform distribution
Central concentration	$n > d+3$	$\frac{n-d-3}{2} > 0$	Concentrated around mean

between particles and maintains particle diversity. This process works as follows: regions with higher particle density have larger values of $\prod_{j=1}^{n} \tilde{\pi}_{i_j}$ in (28), leading to denser sampling in those areas. The spherical interpolation distributes particles over previously unoccupied regions of the ellipsoidal surfaces. Although this does not volumetrically fill the space as in the case of $n > d+1$, it improves particle diversity by creating continuous interpolated surfaces that connect existing particles, rather than being limited to the discrete points that conventional fixed-coefficient merging produces.

5 Theoretical Analysis and Experimental Verification of Merging Dimension

5.1 Theoretical Effects of Merging Dimension on Distribution Characteristics

In the case of $n > d+1$, the effect of merging dimension n on the post-merging particle distribution

$$p(\mathbf{x}_{\text{merged}} \mid X) \propto \left[\frac{n-1}{n} - (\mathbf{x}_{\text{merged}} - \bar{\mathbf{x}})^T (XPX^T)^+ (\mathbf{x}_{\text{merged}} - \bar{\mathbf{x}}) \right]_+^{\frac{n-r-2}{2}} \tag{29}$$

was analyzed based on the probability density of the merged particles. The case $n \leq d+1$ is discussed in section 9.1. Here, $r = \text{rank}(A) \leq d+1$ and $(\mathbf{x}_{\text{merged}} - \bar{\mathbf{x}})^T (XPX^T)^+ (\mathbf{x}_{\text{merged}} - \bar{\mathbf{x}})$ is the squared generalized Mahalanobis distance from the particle mean $\bar{\mathbf{x}}$.

The right-hand side of Eq. (29) determines the distribution shape. Depending on the value of the power exponent $\frac{n-r-2}{2}$, three distinct distribution characteristics emerge. When $n = r+1$, the power exponent becomes negative, and probability density becomes high in regions where the Mahalanobis distance is large, with particles showing edge concentration in the periphery of the distribution. When $n = r+2$, the power exponent becomes zero; hence the density is independent of the Mahalanobis distance and is uniform over the feasible set defined by Eq. (3). When $n > r+2$, the power exponent becomes positive, and the probability density increases in regions with small Mahalanobis distance, exhibiting a tendency to concentrate around $\bar{\mathbf{x}}$.

The theoretical analysis provides distribution properties based on the relationship between merging dimension n and system dimension d. In the case of $r = d+1$, Table 2 summarizes all possible cases and their corresponding distribution characteristics.

https://doi.org/10.5194/egusphere-2026-4073
Preprint. Discussion started: 21 July 2026

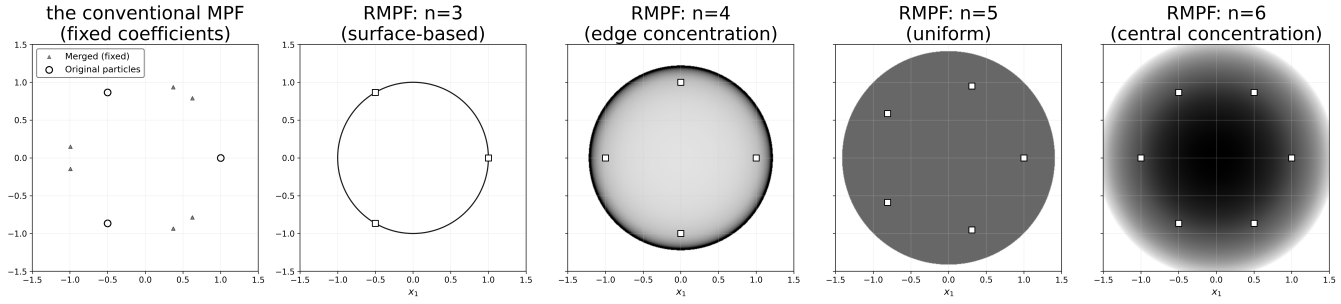

Figure 1. Theoretical densities for conventional MPF and RMPF. Left: Conventional MPF with fixed coefficients (discrete clusters). Right: RMPF theoretical densities for $n = 3, 4, 5, 6$ (continuous distributions on surfaces/volumes). White markers with black edges denote original particles; darker grayscale shading and contour lines indicate higher density.

In the surface-based case ($n \leq d+1$), particles are constrained to $(n-1)$-dimensional ellipsoidal surfaces within the d-dimensional state space, which still allows smoothing the particle approximation in the state space. Continuously sampling merging coefficients populates previously unoccupied regions on those surfaces and preserves diversity. When $n > d+1$, the power exponent $\frac{n-d-3}{2}$ determines the distribution shape: negative exponents yield peripheral concentration; the zero exponent yields a uniform distribution over the feasible region defined by (3); and positive exponents yield central concentration with the density increasing as the Mahalanobis distance to $\bar{\mathbf{x}}$ decreases.

Figure 1 illustrates these theoretical predictions for the two-dimensional case ($d = 2$) with merging dimensions $n = 3, 4, 5, 6$. To highlight the fundamental difference between MPF and RMPF, the leftmost panel shows the distribution produced by the conventional MPF with fixed coefficients, generating only six discrete cluster points from the same three particles arranged on a circle. In contrast, the RMPF panels show continuous theoretical distributions: the surface-based case ($n = 3$) is constrained to a circle (a one-dimensional surface in 2D); the edge-concentration case ($n = 4$) yields higher density near the boundary of the feasible region; the uniform case ($n = 5$) exhibits constant density over the feasible region; and the central-concentration case ($n = 6$) shows a tendency to concentrate around $\bar{\mathbf{x}}$.

The key difference lies in distributional characteristics. Fixed coefficients produce only discrete cluster points, as evidenced by the six isolated points in the leftmost panel, whereas RMPF generates continuous distributions that vary systematically with the merging dimension parameter. All RMPF distributions create merged particles at positions distinct from the original particle locations, and distribution shape can be controlled through the selection of merging dimension n. This classification reveals that the merging dimension provides theoretically predictable control over distribution characteristics.

5.2 Comparison between RMPF and Fixed-Coefficient MPF

To demonstrate the advantages of random merging coefficients over fixed coefficients, numerical experiments were conducted using one-dimensional uniformly spaced particles. The distribution of merged particles of RMPF were compared with those of conventional MPF with fixed coefficients proposed by Nakano et al. (2007).

https://doi.org/10.5194/egusphere-2026-4073
Preprint. Discussion started: 21 July 2026

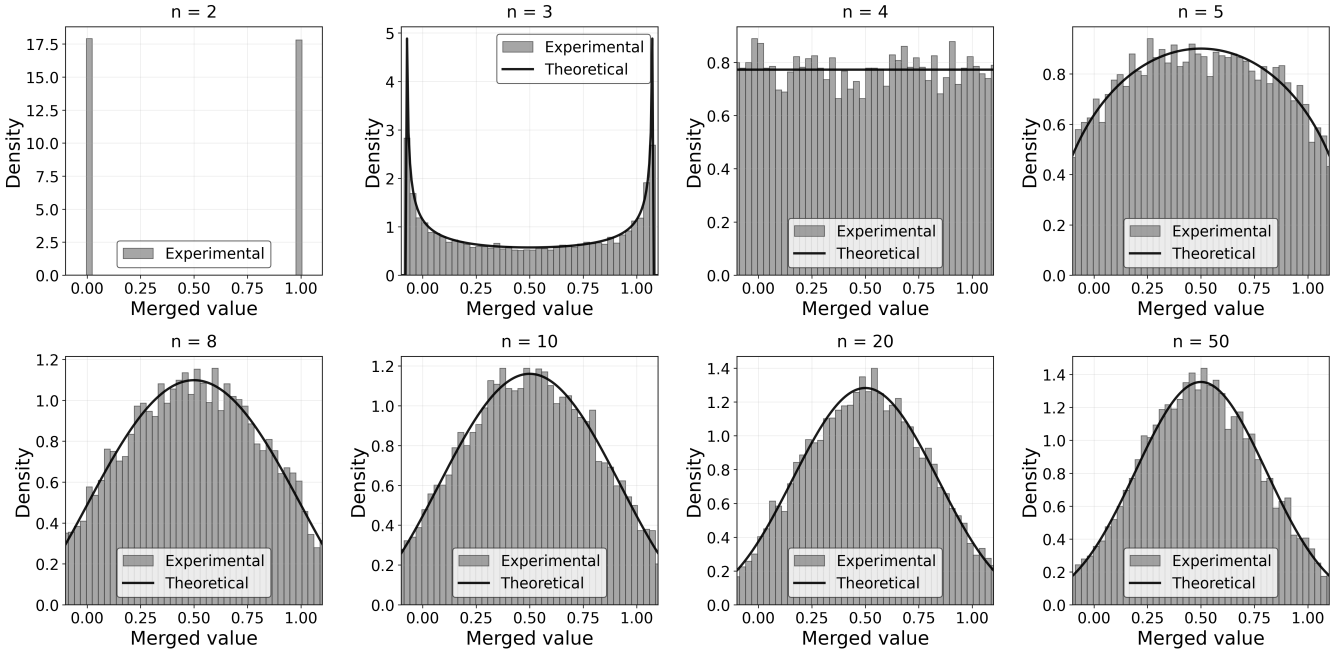

Figure 2. Distribution of merged particles using RMPF with random coefficients in different merging dimensions n. Gray histograms show empirical distributions; black lines represent theoretical densities.

5.2.1 Experimental Setup

For RMPF and conventional MPF, we considered N particles uniformly distributed in the interval $[0,1]$: $X = \{0, \frac{1}{N-1}, \frac{2}{N-1}, \ldots, 1\}$, performing the following procedure 10000 times: randomly select n particles from the set $\mathbf{x}$, generate merging coefficients (either random for RMPF or fixed for MPF), and generate the merged particle as the weighted sum. In these experiments, we set $n = N$ to examine the theoretical distributions for the full merging dimension. This process simulates the merging operation that would occur at each time step in particle filtering.

5.2.2 RMPF with Random Coefficients

Figure 2 shows the distribution of merged particles using RMPF for various merging dimensions, n. The results confirm our theoretical predictions from Section 4. For $n = 2$, only discrete merging is possible with coefficients $(1,0)$ or $(0,1)$, resulting in particles remaining at original positions. As n increases, we observe the predicted transition from edge concentration ($n = 3$, power exponent -0.5) to uniform distribution ($n = 4$, power exponent 0) and then to central concentration ($n \geq 5$, positive power exponent). RMPF generates smooth, continuous distributions that fill the space between the original particles, effectively increasing the resolution of particle representation.

https://doi.org/10.5194/egusphere-2026-4073
Preprint. Discussion started: 21 July 2026

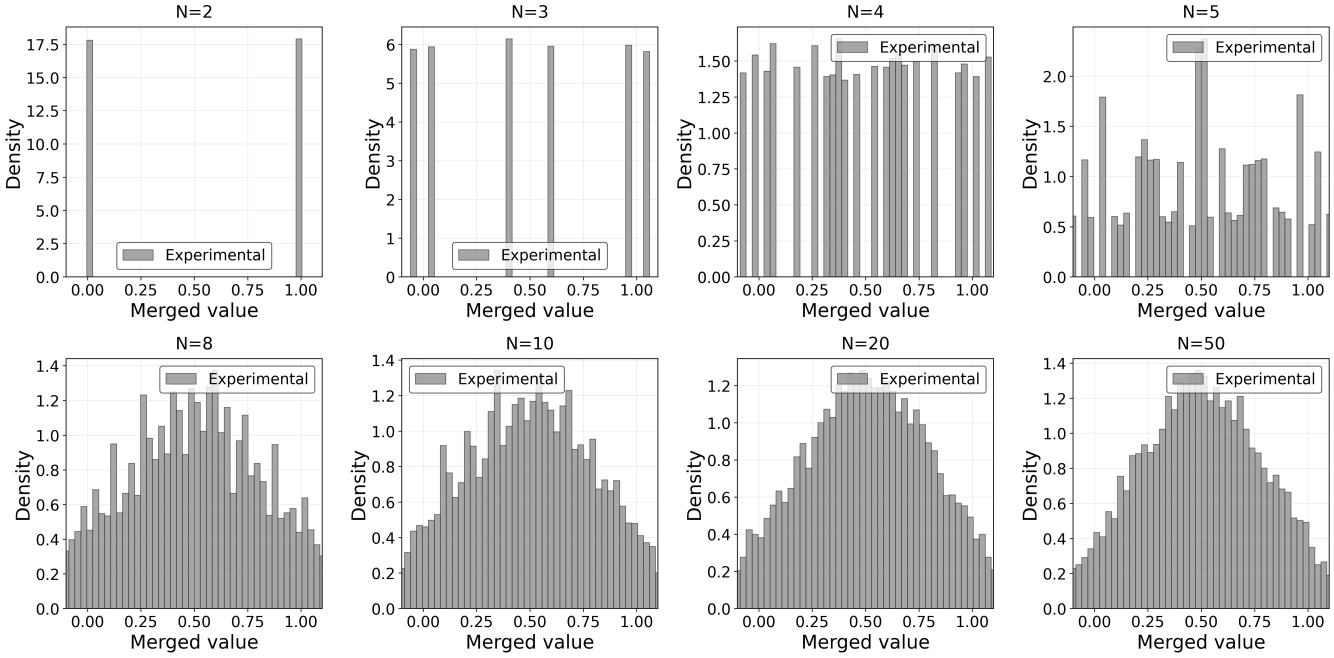

Figure 3. Distribution of merged particles using conventional MPF with fixed coefficients for different values of N particles.

5.2.3 The conventional MPF with Fixed Coefficients

Figure 3 shows the distribution when using the same experimental setup but with fixed coefficients. The following procedure was repeated 10000 times: randomly select three particles from the set $\{0, \frac{1}{N-1}, \frac{2}{N-1}, \ldots, 1\}$ and apply the fixed coefficients $\alpha_1 = \frac{3}{4}$, $\alpha_2 = \frac{\sqrt{13}+1}{8}$, $\alpha_3 = -\frac{\sqrt{13}-1}{8}$ to the selected particles.

The fixed-coefficient MPF produces markedly different results from those of RMPF. Instead of smooth distributions, merged particles appear at a small number of discrete positions determined by the linear combinations of selected particle triplets. As shown in Figure 3, as N increases, the distribution gradually approaches a bell-shaped form more similar to a normal distribution than to what is observed for small N values (e.g., $N = 3$). Nevertheless, the distribution retains inherent biases, with merged particles concentrating at specific discrete positions rather than spreading continuously across the feasible region. This fundamental limitation arises because fixed coefficients can only produce a finite number of possible outcomes (specifically, ${}_N P_n = \frac{N!}{(N-n)!}$ distinct values) from any selected particles, preventing the formation of a truly continuous distribution. The comparison between these two approaches reveals a critical advantage of RMPF. The continuous distributions generated by random coefficients enable effective exploration of the state space between existing particles, whereas fixed coefficients restrict merged particles to discrete positions. This difference affects particle filtering performance. When particle degeneracy occurs and many particles collapse to similar positions, fixed coefficients do not effectively redistribute over the state space, potentially

https://doi.org/10.5194/egusphere-2026-4073
Preprint. Discussion started: 21 July 2026

exacerbating the degeneracy problem. In contrast, RMPF's continuous redistribution maintains particle diversity even when starting from a degenerate configuration.

6 Numerical Experiments with Lorenz63 Model

To verify the theoretical insights derived in the previous section in actual data assimilation systems, we evaluated the performance of RMPF using the Lorenz63 model, which is a standard benchmark in data assimilation research (Lorenz, 1963).

6.1 Experimental Setup

Lorenz63 is the following 3-dimensional chaotic system:

$$\dot{x}_1 = \sigma(x_2 - x_1), \qquad \dot{x}_2 = x_1(\rho - x_3) - x_2, \qquad \dot{x}_3 = x_1 x_2 - \beta x_3, \tag{30}$$

Parameters were set to $\sigma = 10,\ \rho = 28,\ \beta = 8/3$.

Numerical integration over 40000 steps (400 s physical time) was executed using the 4th-order Runge–Kutta method ($\Delta t = 0.01$), with all state variables observed every 20 steps (Gaussian noise with standard deviation 1.0 added). The first 1000 steps were excluded as spin-up, and the remaining 39000 steps were evaluated. Comparison methods included standard PF, MPF with fixed coefficients (three types of representative coefficients (Nakano et al., 2008; Nomura et al., 2019)), and RMPF (merging dimensions $n = 3, 4, 5, 6, 7, 8, 9, 10, 20$), with experiments conducted at 12 levels of particle numbers ranging from $N = 32$ to 65536.

6.2 Experimental Results

6.2.1 Estimation Accuracy (RMSE)

Table 3 shows the average RMSE for each method using different number of particles N. Several important findings were confirmed through these experiments. First, RMPF demonstrates superior performance compared to the conventional MPF when the number of particles is sufficiently large ($N \geq 512$). This improvement is attributed to random merging coefficients, which prevent the distributional bias of fixed-coefficient MPF. However, when the particle number is extremely small ($N \leq 128$), the conventional MPF occasionally outperforms RMPF. This occurs because when the merging dimension is large relative to the particle number, most merging operations in RMPF result in sampling centered around the post-merging estimate, leading to accelerated degeneracy toward the mean. Additionally, the distributional bias that characterizes the weakness of MPF, as noted in Section 5, has less impact in small particle regimes, as RMPF also suffers from irregular behavior when particle numbers are insufficient.

Second, RMPF resolves the RMSE saturation problem that is reported for MPF (Nakano et al., 2007). The method maintains a performance equivalent to that of standard PF even with large particle numbers, and for $N \geq 256$, all methods converge to the RMSE values of 0.234–0.250. The relationship between merging dimension and estimation accuracy showed complex behavior

https://doi.org/10.5194/egusphere-2026-4073
Preprint. Discussion started: 21 July 2026

Table 3. Average RMSE of each method in Lorenz63 model (pre-merging)

ID	Method	Number of particles N								
		32	64	128	256	512	1024	2048	16384	65536
1	$\boldsymbol{\alpha} = [-0.14, 0.16, 0.98]$	9.949	9.975	3.092	1.471	0.253	0.243	0.243	0.242	0.242
2	$\boldsymbol{\alpha} = [0.75, 0.58, -0.33]$	4.256	7.960	0.265	0.259	0.248	0.250	0.247	0.247	0.246
3	$\boldsymbol{\alpha} = [2/3, 2/3, -1/3]$	6.909	1.250	0.255	0.244	0.249	0.246	0.247	0.244	0.245
4	RMPF: $n = 3$	9.728	7.344	7.573	0.240	0.236	0.237	0.234	0.234	0.234
5	RMPF: $n = 4$	9.583	5.871	2.356	0.248	0.235	0.235	0.235	0.235	0.234
6	RMPF: $n = 5$	9.597	4.705	1.550	0.240	0.245	0.238	0.235	0.235	0.235
7	RMPF: $n = 6$	9.715	5.818	1.664	0.252	0.241	0.236	0.237	0.236	0.236
8	RMPF: $n = 7$	10.238	5.556	6.834	0.248	0.235	0.240	0.236	0.236	0.236
9	RMPF: $n = 8$	10.298	5.873	1.159	0.240	0.240	0.238	0.236	0.236	0.236
10	RMPF: $n = 9$	9.970	8.679	1.332	0.245	0.238	0.237	0.236	0.237	0.237
11	RMPF: $n = 10$	9.919	8.808	1.522	0.239	0.237	0.238	0.239	0.237	0.237
12	RMPF: $n = 20$	9.649	6.596	1.326	0.235	0.242	0.238	0.238	0.238	0.238
13	Standard PF	9.942	9.823	10.230	9.211	0.237	0.237	0.237	0.234	0.234

that depends strongly on the number of particles, as illustrated in Figure 4. For small particle numbers ($N = 128$), RMSE generally decreases as merging dimension increases, showing a downward trend that suggests larger merging dimensions are beneficial when particles are scarce. In contrast, for large particle numbers ($N = 8192$), the trend reverses, with RMSE increasing as merging dimension increases, indicating that smaller merging dimensions are preferable when abundant particles are available. The intermediate particle number case ($N = 2048$) exhibits a mixed pattern with relatively stable performance across different merging dimensions, whereas the largest particle number tested ($N = 65536$) shows a slight upward trend similar to the $N = 8192$ case but with much smaller variations in RMSE values.

6.2.2 Effects of Merging Dimension

The selection of merging dimension n showed complex behavior that depended on particle number. With few particles ($N \leq 128$), significant performance differences occur depending on merging dimension selection. For example, at $N = 128$, $n = 8$ achieved the best performance (RMSE=1.159), whereas $n = 3$ showed significant deterioration (RMSE=7.573). For moderate particle numbers ($N = 256$–1024), stable performance is observed across many dimensions, though differences still exist. With large particle numbers ($N \geq 16384$), differences due to merging dimension diminish, with all configurations converging to RMSE values of 0.234–0.238.

The relationship between merging dimension and RMSE exhibited decreasing or monotonic increasing trends depending on the particle number, confirming that the optimal merging dimension varies with the available computational resources. This behavior suggests the possibility of modeling the relationship as a unimodal function, which can enable automatic and efficient

https://doi.org/10.5194/egusphere-2026-4073
Preprint. Discussion started: 21 July 2026

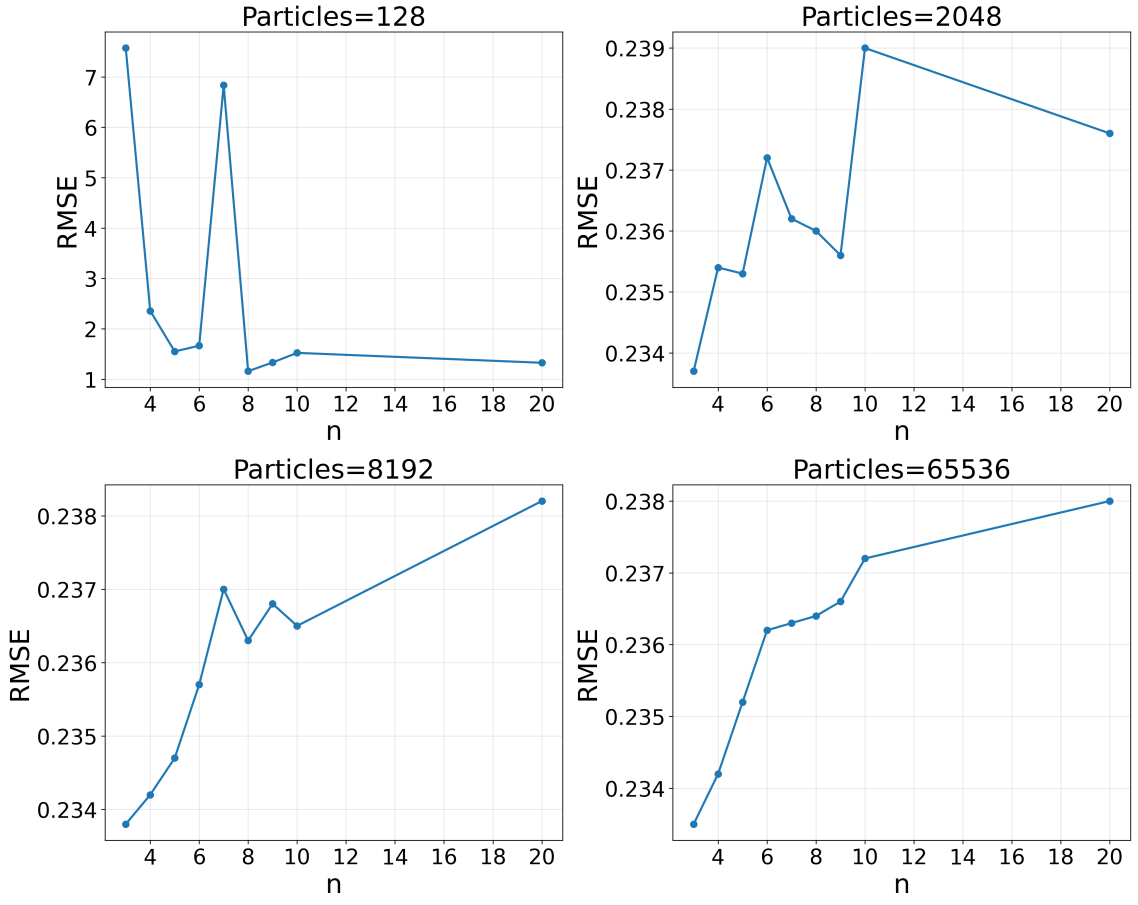

Figure 4. Relationship between merging dimension and RMSE for different numbers of particles in Lorenz63 model.

optimization of merging dimensions through standard optimization techniques. Even small merging dimensions ($n = 3, 4, 5$) relative to the system dimension ($d = 3$) demonstrated significant improvements over standard PF, indicating that RMPF is effective even when $n < d + 1$. Although optimal dimensions vary according to particle number, the method consistently outperformed conventional approaches across a wide range of merging dimensions, making it particularly suitable for high-dimensional systems where $n \gg d$ is computationally prohibitive.

6.2.3 Comparison of Pre- and Post-merging Estimation Accuracy

Table 4 compares RMSE for pre-merging and post-merging steps. Pre-merging estimates are superior for all merging-type methods, confirming the effectiveness of the approach. While merging operations cause an average 7-10% information loss, the adaptive sampling characteristics achieve high-accuracy estimation with few particles and approach the limiting performance of standard PF with large particles.

https://doi.org/10.5194/egusphere-2026-4073
Preprint. Discussion started: 21 July 2026

Table 4. Comparison of average RMSE calculated at pre-merging and post-merging steps

Method	$N = 256$		$N = 16384$	
	Pre-merging	Post-merging	Pre-merging	Post-merging
$\boldsymbol{\alpha} = [-0.14, 0.16, 0.98]$	1.471	1.481	0.242	0.263
$\boldsymbol{\alpha} = [0.75, 0.58, -0.33]$	0.259	0.280	0.247	0.272
$\boldsymbol{\alpha} = [2/3, 2/3, -1/3]$	0.244	0.267	0.244	0.269
RMPF: $n = 3$	0.240	0.254	0.234	0.251
RMPF: $n = 4$	0.248	0.261	0.235	0.251
RMPF: $n = 5$	0.240	0.254	0.235	0.252
RMPF: $n = 6$	0.252	0.268	0.236	0.253
RMPF: $n = 7$	0.248	0.261	0.236	0.253
RMPF: $n = 8$	0.240	0.253	0.236	0.253
RMPF: $n = 9$	0.245	0.258	0.237	0.254
RMPF: $n = 10$	0.239	0.253	0.237	0.254
RMPF: $n = 20$	0.235	0.250	0.238	0.255

7 Numerical Experiments with Lorenz96 Model

After Lorenz63 (3-dimensional) reported in the previous chapter, we conducted experiments using the 40-dimensional Lorenz96 model to verify the effectiveness of RMPF in higher-dimensional systems (Lorenz, 1996).

7.1 Experimental Setup

Lorenz96 is the following 40-dimensional chaotic system:

$$\frac{dx_j}{dt} = (x_{j+1} - x_{j-2})x_{j-1} - x_j + F, \quad j = 1, \ldots, 40 \tag{31}$$

Setting $F = 8$ under periodic boundary conditions, integration was performed for 20000 steps with time step $\Delta t = 0.005$, excluding the first 2000 steps as spin-up. Observations targeted only even-indexed variables $\{x_2, x_4, \ldots, x_{40}\}$ every 10 steps, adding Gaussian noise of standard deviation 1.5. This simulates a practical setting where only half of the state variables are observable. The comparison methods were the same as those of Lorenz63 (standard PF, three types of fixed MPF, RMPF), with merging dimensions verified at $n = 3, 5, 10, 20, 30, 35, 37\text{–}45, 80, 100$, focusing on values around the system dimension $d = 40$. Experiments were conducted at eight levels of particle numbers in the range of $N = 128$ to $N = 262144$.

7.2 Experimental Results

7.2.1 Estimation Accuracy (RMSE)

Table 5 shows the average RMSE for each method.

https://doi.org/10.5194/egusphere-2026-4073
Preprint. Discussion started: 21 July 2026

Table 5. Average RMSE of each method in Lorenz96 model (pre-merging)

ID	Method	Number of particles N							
		128	1024	4096	8192	16384	65536	131072	262144
1	$\boldsymbol{\alpha} = [-0.14, 0.16, 0.98]$	4.642	3.973	3.774	3.506	3.519	3.033	2.899	2.738
2	$\boldsymbol{\alpha} = [0.75, 0.58, -0.33]$	4.537	4.071	3.700	3.531	3.290	3.159	2.852	2.638
3	$\boldsymbol{\alpha} = [2/3, 2/3, -1/3]$	4.479	4.041	3.592	3.526	3.511	3.221	2.830	2.678
4	RMPF: $n = 3$	4.528	4.067	3.654	3.559	3.365	3.074	2.931	2.558
5	RMPF: $n = 5$	4.588	3.979	3.701	3.557	3.323	2.952	2.824	2.769
6	RMPF: $n = 10$	4.484	3.926	3.608	3.439	3.264	2.939	2.818	2.537
7	RMPF: $n = 20$	4.545	3.952	3.621	3.355	3.149	2.808	2.672	2.547
8	RMPF: $n = 30$	4.538	3.830	3.495	3.271	3.175	2.621	2.422	2.287
9	RMPF: $n = 35$	4.345	3.898	3.414	3.222	3.030	2.725	2.670	2.314
10	RMPF: $n = 37$	4.282	3.848	3.397	3.423	3.117	2.741	2.501	2.245
11	RMPF: $n = 38$	4.381	3.906	3.533	3.338	3.213	2.730	2.475	2.288
12	RMPF: $n = 39$	4.444	3.877	3.417	3.206	3.129	2.537	2.545	2.260
13	RMPF: $n = 40$	4.454	3.748	3.257	3.347	3.069	2.740	2.475	2.097
14	RMPF: $n = 41$	4.344	3.776	3.564	3.244	3.093	2.798	2.539	2.173
15	RMPF: $n = 42$	4.299	3.847	3.477	3.324	3.197	2.673	2.333	2.252
16	RMPF: $n = 43$	4.364	3.670	3.490	3.251	3.116	2.612	2.524	2.293
17	RMPF: $n = 44$	4.316	3.775	3.399	3.193	2.989	2.641	2.417	2.285
18	RMPF: $n = 45$	4.256	3.624	3.318	3.204	3.213	2.688	2.468	2.094
19	RMPF: $n = 80$	4.326	3.679	3.463	3.250	2.986	2.420	2.319	2.178
20	RMPF: $n = 100$	4.324	3.701	3.332	3.211	2.798	2.392	2.198	2.139
21	Standard PF	4.677	4.057	3.679	3.561	3.408	2.997	2.771	2.704

Compared to standard PF, RMPF showed superior performance, particularly in the large particle number regime ($N \geq 65536$). At $N = 262144$, configurations with $n = 40, 45$ achieved RMSE values of 2.09–2.10, representing approximately 22% improvement over standard PF (2.70). A notable relationship with system dimension was observed, with settings of $n \geq 40$ (above the system dimension of 40) showing consistently good results.

The selection of the merging dimension showed systematic behavior in Lorenz96. As illustrated in Figure 5 and summarized in Table 5, RMSE decreases as n increases across all tested particle numbers, with the trend being particularly pronounced for larger N ($N = 8192, 65536$). Around $n \approx d$ (i.e., near the state dimension), RMSE exhibits sharp fluctuations and appears unstable, whereas improvements are obtained over standard PF with small n ($n = 3, 5, 10, 20$). From a computational perspective, modest improvements at smaller n remain attractive for ultra–high-dimensional applications where $n \ll d$ is unavoidable. Overall, RMPF was effective over a wide range of n, enabling application-specific trade-offs between cost and accuracy.

https://doi.org/10.5194/egusphere-2026-4073
Preprint. Discussion started: 21 July 2026

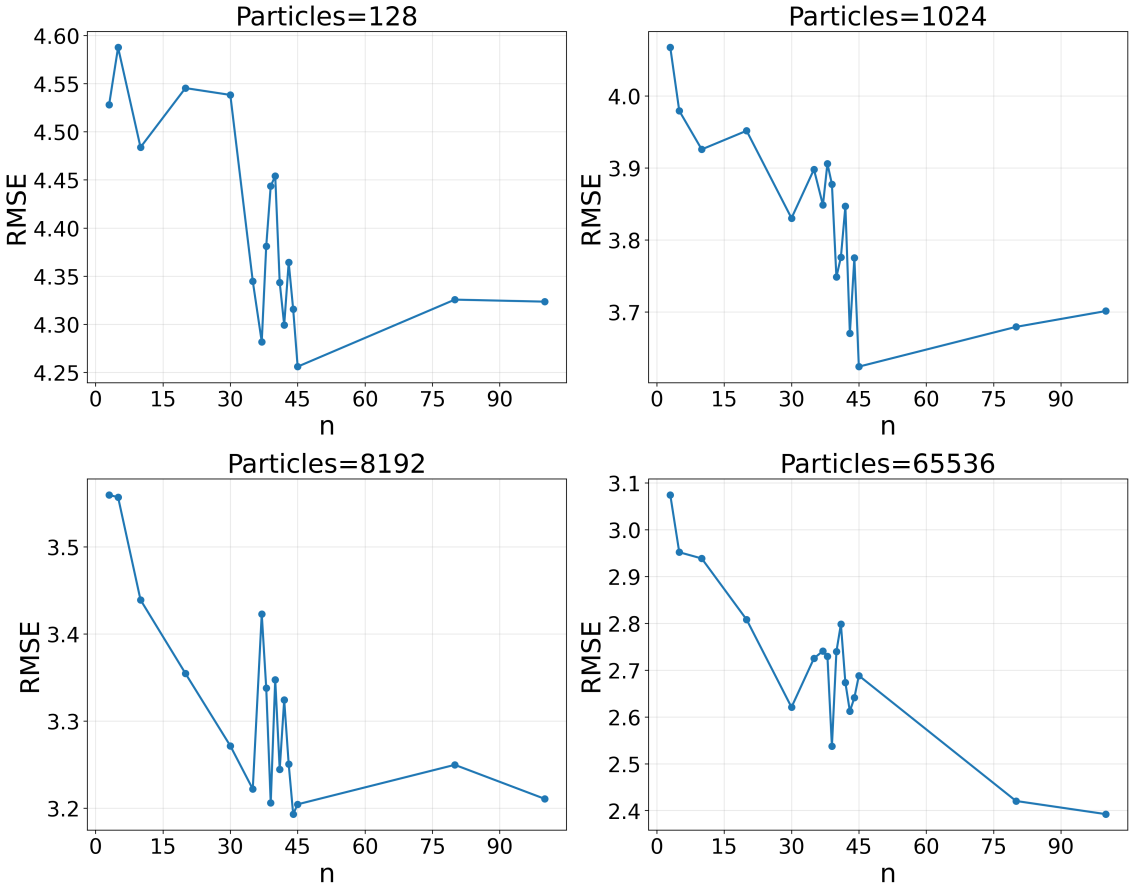

Figure 5. Relationship between merging dimension and RMSE for different numbers of particles in the Lorenz96 model. The plots show how RMSE varies with the merging dimension for four different particle numbers N: 128, 1024, 8192, and 65536. Each subplot demonstrates the performance characteristics of the RMPF method across different n settings.

Table 6. Comparison of particle numbers required for equivalent RMSE achievement

Method	Required particles	RMSE
Standard PF	2^{18}	2.70
Fixed MPF ($\boldsymbol{\alpha} = [0.75, 0.58, -0.33]$)	2^{18}	2.64
RMPF ($n = 40$)	2^{16}	2.74
RMPF ($n = 45$)	2^{16}	2.69
RMPF ($n = 100$)	2^{15}	2.77

Table 6 shows the particle numbers required to achieve an RMSE of 2.8 or lower. The RMPF achieved equivalent accuracy with $1/4$ to $1/8$ the number of particles required by the standard PF. In particular, with $n = 100$, the reduction in particle number was about $1/8$, which is significant for high-cost, large-scale systems.

https://doi.org/10.5194/egusphere-2026-4073
Preprint. Discussion started: 21 July 2026

Table 7. Comparison of average RMSE calculated at pre-merging and post-merging steps.

Method	$N = 131072$		$N = 262144$	
	Pre-merging	Post-merging	Pre-merging	Post-merging
$\boldsymbol{\alpha} = [-0.14, 0.16, 0.98]$	2.90	3.08	2.74	2.96
$\boldsymbol{\alpha} = [0.75, 0.58, -0.33]$	2.85	3.05	2.64	2.87
$\boldsymbol{\alpha} = [2/3, 2/3, -1/3]$	2.83	3.02	2.68	2.89
RMPF: $n = 40$	2.48	2.67	2.10	2.33
RMPF: $n = 42$	2.33	2.54	2.25	2.49
RMPF: $n = 45$	2.47	2.66	2.09	2.34
RMPF: $n = 100$	2.20	2.38	2.14	2.35

These results reveal complex behavior dependent on merging dimension and particle number. Unlike the Lorenz63 model, the Lorenz96 model demonstrates a monotonic decreasing relationship between merging dimension and RMSE across all tested particle numbers. Although smaller merging dimensions ($n = 3, 5, 10, 20$) show improvements compared to standard PF, particularly evident at higher particle numbers ($N \geq 65536$), the most consistent and substantial improvements are observed with larger dimensions ($n \geq 40$). For instance, at $N = 262144$, configurations with $n = 40, 45$ achieved RMSE values of 2.09-2.10, representing approximately 22% improvement over standard PF (2.70). However, from a computational efficiency perspective, even modest improvements with smaller n values become highly valuable for ultra-high-dimensional systems encountered in meteorological and oceanographic data assimilation, where computational constraints necessitate $n \ll d$ and state dimensions can reach millions.

7.2.2 Comparison of Pre- and Post-merging Estimation Accuracy

Table 7 shows a comparison of RMSE calculated at pre-merging and post-merging steps.

Similar to Lorenz63, pre-merging estimates are superior to post-merging estimates for all methods, with an average improvement of 7-9%. This demonstrates that the effectiveness of the pre-merging approach is maintained even as system dimension increases. To visualize the smoothing effects underlying these numerical results, Figure 6 shows the particle distributions at pre-merging and post-merging steps for different merging dimensions at a specific time point ($t = 1000$) for the Lorenz96 model. Figure 6 clearly demonstrates the mechanism behind the accuracy differences observed in Table 7. The pre-merging distributions (left panels) preserve the detailed structure of the particle ensemble obtained from observations, maintaining particle diversity. In contrast, the post-merging distributions (right panels) show strong smoothing effects as the merging dimension grows from $n = 3$ to $n = 80$. This smoothing reduces particle degeneracy and improves exploration at subsequent time steps; however, it inevitably results in some information loss for the pre-merging estimate, explaining why pre-merging estimates consistently outperform post-merging estimates across all configurations.

https://doi.org/10.5194/egusphere-2026-4073
Preprint. Discussion started: 21 July 2026

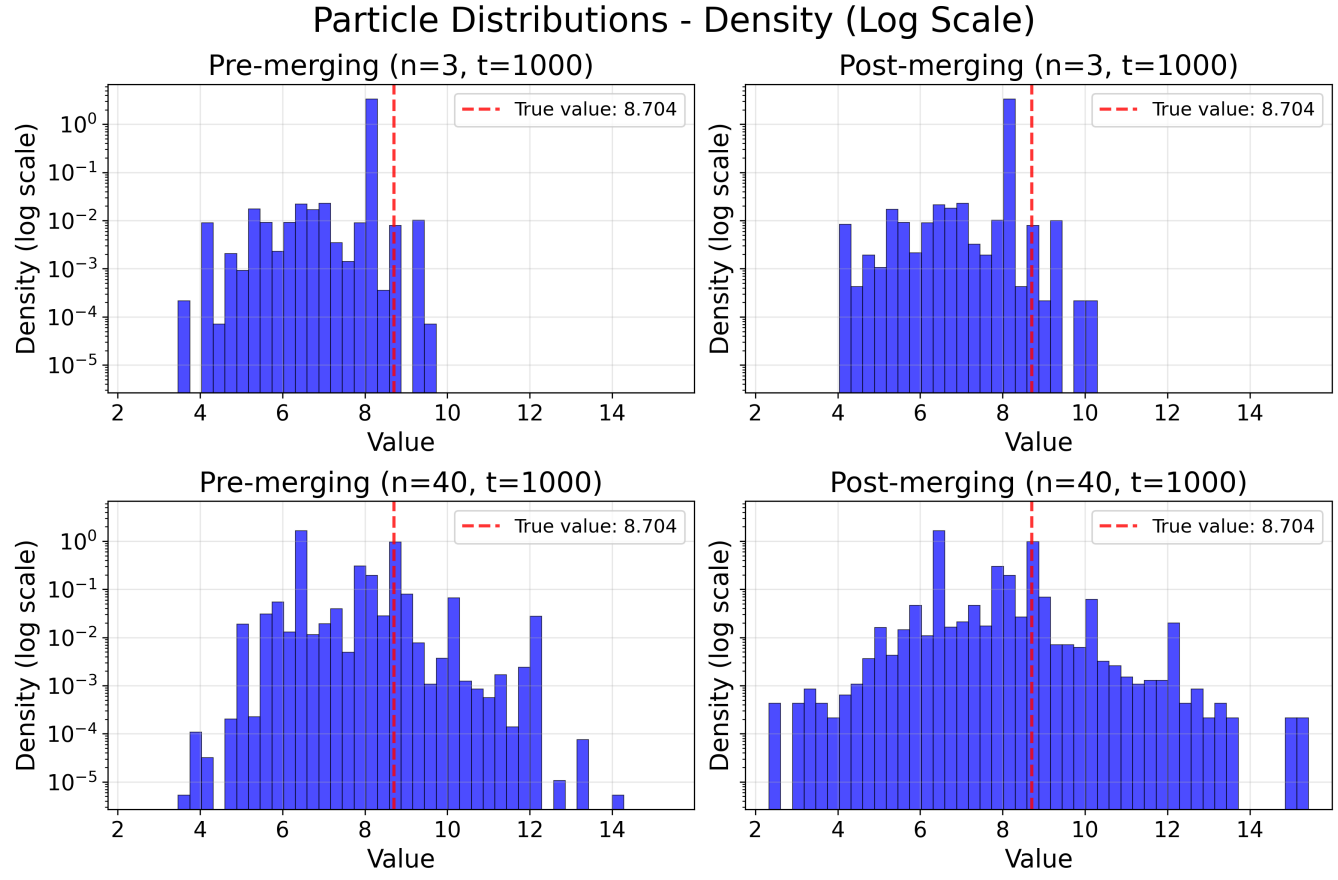

Figure 6. Comparison of particle distributions at pre-merging and post-merging step for different merging dimensions ($n = 3, 40, 80$) at $t = 1000$ in Lorenz96 model.

This evidence reinforces the theoretical foundation of the RMPF approach: the merging operation primarily acts as a regularization mechanism to enhance particle diversity, and the actual state estimation is performed using the pre-merging distribution, which retains the information most observable.

8 Practical Merging Dimension Selection: Likelihood Maximization Approach

The experiments reported in the previous sections confirm that the selection of the merging dimension n significantly affects estimation accuracy. However, in practical applications, the true state is unknown, making optimization based on RMSE impossible. Before introducing a likelihood-based criterion, we first describe why the choice of n can be interpreted as a bias–variance trade-off in terms of the mean integrated squared error (MISE) of the merged-particle distribution.

https://doi.org/10.5194/egusphere-2026-4073
Preprint. Discussion started: 21 July 2026

8.1 MISE-type interpretation of the role of merging dimension

Let $p_t(\mathbf{x}) = p(\mathbf{x}_t = \mathbf{x} \mid \mathbf{y}_{1:t})$ denote the filtering density at time t. For a fixed weighted particle cloud $\{(\mathbf{x}_t^{(i)}, \tilde{\pi}_t^{(i)})\}_{i=1}^N$, the RMPF merging operation induces a generative density for one merged particle. Using the notation of Section 5, this density can be written as

$$\begin{aligned} q_{t,n,N}(\mathbf{x}) &= \sum_{I \in [N]^n} P(I \mid \tilde{\boldsymbol{\pi}}_t)\, p(\mathbf{x} \mid X_I), \\ P(I \mid \tilde{\boldsymbol{\pi}}_t) &= \prod_{j=1}^{n} \tilde{\pi}_t^{(i_j)}, \end{aligned} \tag{32}$$

where $I = (i_1, \ldots, i_n)$ is an index tuple of the parent particles and $X_I = (\mathbf{x}_t^{(i_1)}, \ldots, \mathbf{x}_t^{(i_n)})$ is the corresponding particle matrix. The discrepancy introduced by the merging operation can then be described by the MISE-type quantity

$$\mathcal{E}_t(n,N) = \mathbb{E}\left[\int \{q_{t,n,N}(\mathbf{x}) - p_t(\mathbf{x})\}^2 \, d\mathbf{x}\right]. \tag{33}$$

Let $q_{t,n}$ denote the population merged density obtained by replacing the finite weighted particle cloud with the exact filtering distribution. Then Eq. (33) admits the standard bias–variance decomposition

$$\begin{aligned} \mathcal{E}_t(n,N) = \|q_{t,n} - p_t\|_{L^2}^2 &+ \mathbb{E}\left[\|q_{t,n,N} - q_{t,n}\|_{L^2}^2\right] \\ &+ 2\mathbb{E}\left[\langle q_{t,n,N} - q_{t,n}, q_{t,n} - p_t \rangle_{L^2}\right]. \end{aligned} \tag{34}$$

Under the idealized sampling interpretation, the last cross term vanishes when $\mathbb{E}[q_{t,n,N}] = q_{t,n}$, and it is treated as negligible in the following qualitative discussion. The first term in Eq. (34) represents the distributional shape bias induced by the merging kernel, whereas the second term represents the finite-particle and group-sampling variability.

The theoretical density derived in Section 5 shows that the merging dimension n controls the shape of the compact-support kernel. In particular, when $n > r + 1$, the conditional density of a merged particle has the form

$$p(\mathbf{x}_{\text{merged}} \mid X) \propto \left[R^2(\mathbf{x}_{\text{merged}})\right]_+^{(n-r-2)/2}, \tag{35}$$

where $r = \operatorname{rank}(A)$ is the effective rank of the augmented system. Thus, for fixed r, increasing n changes the kernel from boundary-concentrated to uniform and then to centrally concentrated. This operation can be interpreted as increasing the smoothing or Gaussianizing strength of the merging step. We summarize this effect by a coefficient $\lambda_{n,r} \in [0,1]$, which represents the extent to which the merged-particle density is pulled toward a Gaussian-like moment-preserving approximation. If

$$\Delta_{2,t} = \|\phi(\cdot; \boldsymbol{\mu}_t, \boldsymbol{\Sigma}_t) - p_t\|_{L^2}, \tag{36}$$

where $\phi(\cdot; \boldsymbol{\mu}_t, \boldsymbol{\Sigma}_t)$ is the Gaussian density with the same first two moments as p_t, then the shape-bias term can be heuristically represented as

$$\|q_{t,n} - p_t\|_{L^2}^2 \approx \lambda_{n,r}^2 \Delta_{2,t}^2. \tag{37}$$

https://doi.org/10.5194/egusphere-2026-4073
Preprint. Discussion started: 21 July 2026

The variance component can be interpreted through the large-n behavior of the randomly selected parent group. Suppose that the parent indices $I = (i_1, \ldots, i_n)$ are sampled with replacement from the weighted empirical measure defined by $\{(\mathbf{x}_t^{(i)}, \tilde{\pi}_t^{(i)})\}_{i=1}^N$. Let

$$\boldsymbol{\mu}_{\tilde{\pi},t} = \sum_{i=1}^{N} \tilde{\pi}_t^{(i)} \mathbf{x}_t^{(i)},$$
$$\boldsymbol{\Sigma}_{\tilde{\pi},t} = \sum_{i=1}^{N} \tilde{\pi}_t^{(i)} (\mathbf{x}_t^{(i)} - \boldsymbol{\mu}_{\tilde{\pi},t})(\mathbf{x}_t^{(i)} - \boldsymbol{\mu}_{\tilde{\pi},t})^\top.$$

Then, as n becomes large, the empirical mean and covariance of the selected parent group satisfy

$$\bar{\mathbf{x}}_I = \frac{1}{n} \sum_{j=1}^{n} \mathbf{x}_t^{(i_j)} = \boldsymbol{\mu}_{\tilde{\pi},t} + O_p(n^{-1/2}), \tag{38}$$

$$\frac{1}{n} X_I P X_I^\top = \boldsymbol{\Sigma}_{\tilde{\pi},t} + O_p(n^{-1/2}), \tag{39}$$

where $P = I_n - n^{-1}\mathbf{1}_n\mathbf{1}_n^\top$. Therefore, for large n, the conditional merging density $p(\mathbf{x} \mid X_I)$ fluctuates around its population counterpart mainly through the $O_p(n^{-1/2})$ fluctuations of the empirical center and covariance of the selected parent group. Consequently, the integrated squared fluctuation of the induced density is expected to be of order $O(1/n)$, and the variance component in Eq. (34) can be summarized by the approximation

$$\mathbb{E}\left[\|q_{t,n,N} - q_{t,n}\|_{L^2}^2\right] \approx \frac{C_t(N)}{n}, \tag{40}$$

where $C_t(N)$ absorbs the finite-particle variability, the local sensitivity of the merging kernel, and the dependence on the weighted empirical distribution.

Combining the bias term in Eq. (37) with the variance term in Eq. (40), the MISE can be summarized by the proxy

$$\mathcal{E}_t(n, N) \approx \lambda_{n,r}^2 \Delta_{2,t}^2 + \frac{C_t(N)}{n}. \tag{41}$$

Equation (41) explains why the optimal merging dimension is not universal, as illustrated conceptually in Fig. 7. The two terms act in opposite directions as n grows: the variance term $C_t(N)/n$ decreases monotonically, while the shape-bias term $\lambda_{n,r}^2 \Delta_{2,t}^2$ increases monotonically and saturates at the plateau $\Delta_{2,t}^2$, reflecting the progressive Gaussianization of the merging kernel. A small n may leave substantial Monte Carlo variation in the merged-particle distribution, whereas an excessively large n can over-smooth the filtering density and increase the shape bias, especially when p_t is strongly non-Gaussian or multimodal. The sum of the two terms is therefore minimized at an interior optimum $n^\star$, so the selection of n should be treated as a problem-dependent bias–variance trade-off rather than as a fixed rule based only on the state dimension. Because p_t and $\Delta_{2,t}$ are unknown in practical applications, Eq. (41) cannot be minimized directly. This motivates the use of an observable proxy criterion, namely the predictive log-likelihood, as described next.

https://doi.org/10.5194/egusphere-2026-4073
Preprint. Discussion started: 21 July 2026

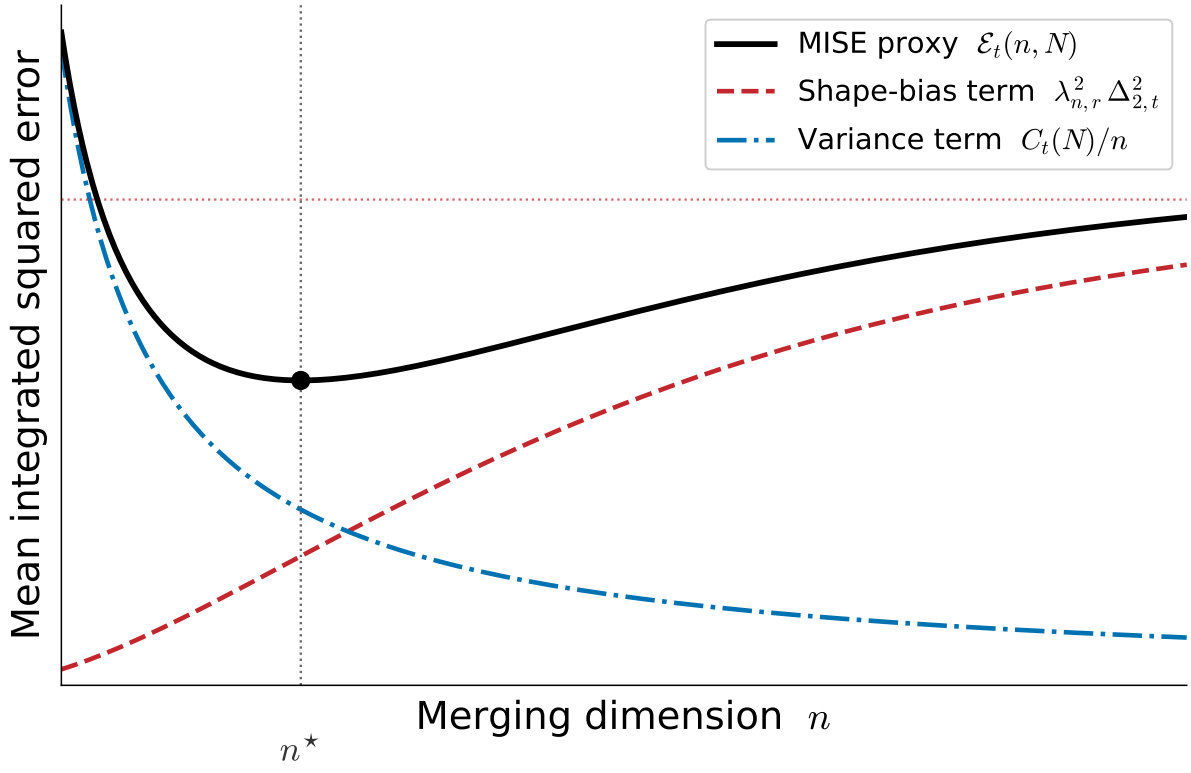

Figure 7. Conceptual illustration of the MISE proxy in Eq. (41) as a function of the merging dimension n. The shape-bias term $\lambda_{n,r}^2 \Delta_{2,t}^2$ (red dashed) increases monotonically and saturates at the plateau $\Delta_{2,t}^2$ (horizontal dotted line) as the merging kernel is pulled toward a Gaussian-like moment-preserving approximation, whereas the variance term $C_t(N)/n$ (blue dash-dotted) decreases monotonically. Their sum, the MISE proxy $\mathcal{E}_t(n, N)$ (black solid), forms a bias–variance trade-off curve with an interior optimum at $n^\star$. The vertical scale is in arbitrary units, and the curves are drawn only to convey the qualitative shapes.

8.2 Relationship Between Likelihood and Estimation Error

The log-likelihood calculated at the resampling step can be utilized as a criterion for selecting parameters in particle filters. We summarize the aggregation as

$$\hat{L} = \sum_{t=t_0}^{T} \hat{\ell}_t, \qquad \bar{\ell} = \frac{1}{T - t_0 + 1} \sum_{t=t_0}^{T} \hat{\ell}_t, \tag{42}$$

where $\hat{\ell}_t$ denotes the per–time-step log-likelihood at time t. The log-score is a strictly proper scoring rule, meaning that its expected value is maximized when the predictive distribution coincides with the true data-generating distribution (Gneiting and Raftery, 2007; Fan, 2016; Douc et al., 2004). Since the number of parameters is fixed in the present setting, information criteria such as the Akaike information criterion (AIC) or Bayesian information criterion (BIC) are unnecessary, and direct comparison of the average log-likelihoods is sufficient. In related studies on PF-based fault detection, the log-likelihood has

https://doi.org/10.5194/egusphere-2026-4073
Preprint. Discussion started: 21 July 2026

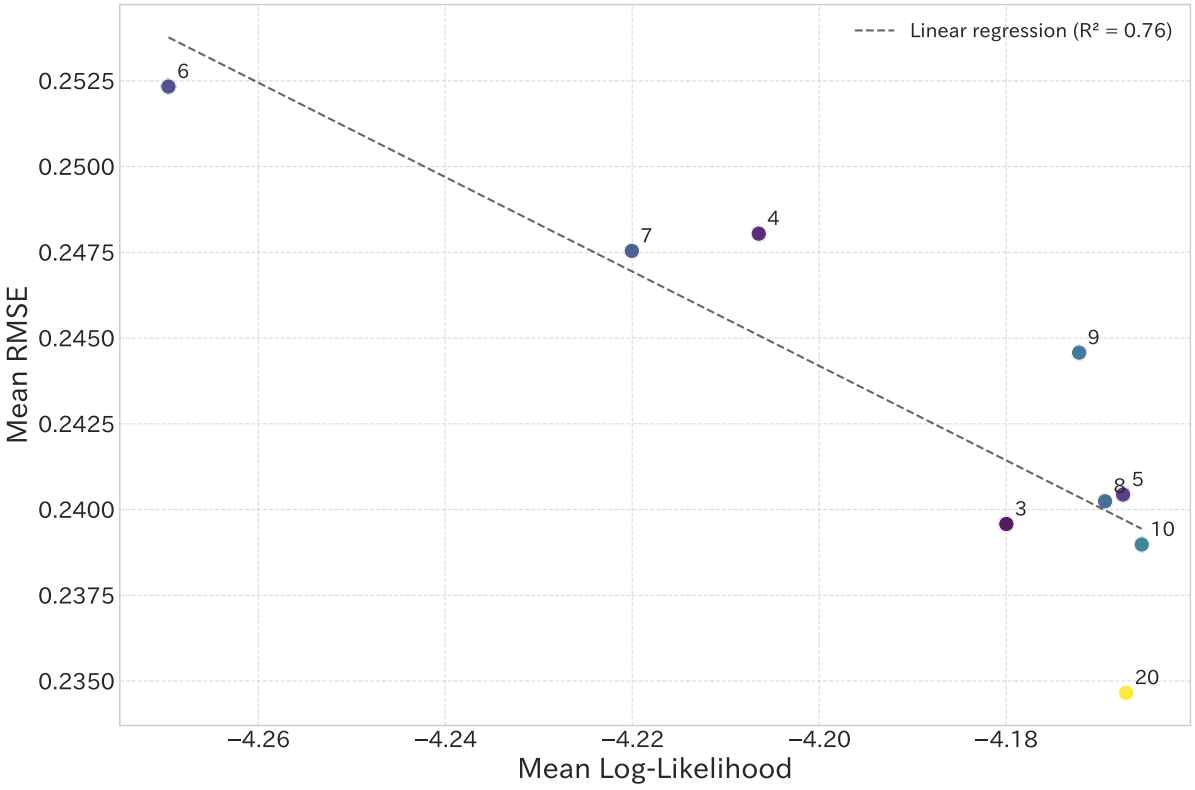

Figure 8. Relationship between mean log-likelihood and mean RMSE in Lorenz63 model (particle number $N = 256$). Superscript next to each point indicates the merging dimension n.

been compared with other potential indicators, including the effective sample size, entropy of particle weights, Kullback–Leibler divergence, the Bhattacharyya distance. Empirical evaluations have shown that the log-likelihood is often the most practical and discriminative measure for detecting changes in system behavior, offering clear thresholds and robust performance in various scenarios (Darányi and Abonyi, 2024; Kenyeres and Abonyi, 2023).

Figures 8 and 9 show the relationship between average log-likelihood and average RMSE for each model. The horizontal axis shows the average pre-merging log-likelihood $\bar{\ell} = \frac{1}{T'} \sum_{t>t_0} \hat{\ell}_t$ with the per–time-step log-likelihood $\hat{\ell}_t = \log\left(\frac{1}{N} \sum_{i=1}^{N} \pi_t^i\right)$, where $\pi_t^i := p\left(\mathbf{y}_t \mid \mathbf{x}_t^{(i)}\right)$ is the likelihood (unnormalized importance weight) of particle i at time t, and $T' = T - t_0$ is the number of evaluated steps.

Strong negative correlations between log-likelihood and RMSE were confirmed in both. This indicates that likelihood maximization is approximately equivalent to RMSE minimization. As an important finding, the merging dimensions showing the highest likelihood matched those achieving minimum RMSE in both models. Lorenz63 obtained the best results at $n = 20$, and Lorenz96 at $n = 45$; both are larger values than the system dimensions ($d = 3$ and $d = 40$). Additionally, in high-dimensional

https://doi.org/10.5194/egusphere-2026-4073
Preprint. Discussion started: 21 July 2026

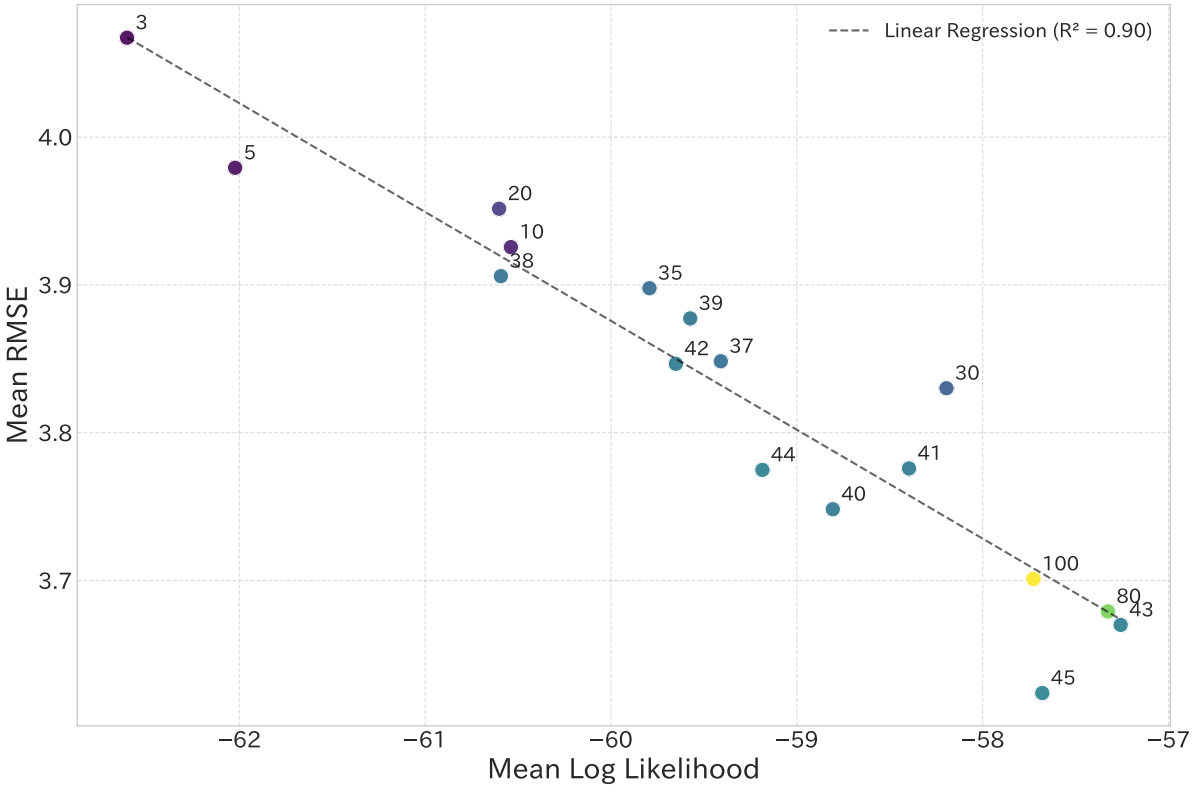

Figure 9. Relationship between average log-likelihood and average RMSE in Lorenz96 model (particle number $N = 1024$). Superscript next to each point indicates the merging dimension n.

systems (Lorenz96), the relationship between likelihood and RMSE shows stronger linearity, suggesting that the reliability of the likelihood maximization approach improves at high dimensions.

8.3 Practical Selection Guidelines

The numerical experiments provide several key insights into merging dimension selection. The effectiveness of likelihood maximization is clearly demonstrated, with log-likelihood functioning as a practical proxy indicator for estimation accuracy. Rather than following a universal rule for merging dimension selection, the optimal choice of n depends significantly on the specific properties of each problem, including system dimensionality, computational constraints, observation conditions such as partial observation scenarios, and noise levels. The reliability of the likelihood maximization approach improved in high dimensions, as the relationship between likelihood and RMSE becomes more linear, enhancing selection reliability. This emphasizes the importance of adaptive selection strategies that consider the trade-off between computational efficiency and estimation accuracy for each specific application, making RMPF particularly versatile for diverse data assimilation scenarios ranging from low-dimensional laboratory systems to ultra-high-dimensional operational models.

https://doi.org/10.5194/egusphere-2026-4073
Preprint. Discussion started: 21 July 2026

9 Discussion

9.1 Improvement mechanism of RMPF

n denotes the *merging dimension* (the number of source particles combined to form one merged particle), and d denotes the *state dimension*. (Here $r = \mathrm{rank}(A) = \min(n, d+1)$ is the rank of the augmented matrix $A = [\mathbf{1}_n^\top; X]$ introduced in Section 4, consistent with Eq. (24) and Table 2; the squared Mahalanobis term then lives on an ellipsoid of dimension $k = r - 1 = \mathrm{rank}(XPX^\top) = \min(n-1, d)$.) The analysis in Section 5 considered the case $n > d+1$, for which a detailed probability–density treatment is available. Our results show that RMPF performs kernel-like smoothing via particle merging, which is conceptually akin to Gaussian-kernel density estimation (Davis et al., 2011; Parzen, 1962). Specifically, the probability density of a merged particle is

$$p(\mathbf{x}_{\mathrm{merged}} \mid X) = C_{n,r} \left|\det{}'(XPX^\top)\right|^{-1/2} \times [R^2(\mathbf{x}_{\mathrm{merged}})]_+^{\frac{n-r-2}{2}}, \tag{43}$$

where $R^2 = \frac{n-1}{n} - (\mathbf{x}_{\mathrm{merged}} - \bar{\mathbf{x}})^\top (XPX^\top)^+ (\mathbf{x}_{\mathrm{merged}} - \bar{\mathbf{x}})$ and $[\cdot]_+ = \max(\cdot, 0)$. Within the ellipsoidal support $\{x : R^2(x) \geq 0\}$, the kernel shape is a compact-support polynomial $(a - \|t\|^2)^\beta$ with $\beta = \frac{1}{2}(n - r - 2)$. Hence n governs boundary concentration ($n < r+2$), uniform interior ($n = r+2$), and central concentration ($n > r+2$). Increasing n raises β and strengthens the concentration near $\bar{\mathbf{x}}$ in the Mahalanobis geometry; moreover, by the law-of-large-numbers/central limit theorem (CLT) argument, $\bar{\mathbf{x}}$ (the mean of the n selected particles) converges to the overall ensemble mean $\boldsymbol{\mu}_X := \sum_{i=1}^N \tilde{\pi}_i \mathbf{x}^{(i)}$ as $n \to \infty$.

This kernel-mixture viewpoint matches the observed behavior in both benchmarks. For Lorenz63 ($d = 3$), Figure 1 shows the transition from surface-based to volumetric cases, and Tables 3–4 (e.g., Table 3) show that (i) RMPF alleviates the RMSE saturation of the conventional MPF at large N, and (ii) the optimal n depends on the particle budget N (Fig. 4). For small N, larger n induces stronger regularization; for large N, overly large n can over-smooth and slightly degrade RMSE, which is consistent with β acting as a "smoothing knob." In Lorenz96 ($d = 40$), Table 5 and Fig. 5 indicate a near-monotonic RMSE decrease as n increases (for fixed N), and Table 6 shows that RMPF attains PF-level accuracy with $\frac{1}{4}$ to $\frac{1}{8}$ of the particles when $n \gtrsim d$ (e.g., $n = 40, 45, 100$). These trends corroborate the theory that effective smoothing strength and exploration in higher dimensions improve with larger n.

In the case of $n \leq d+1$ (surface-based resampling), feasible states lie on $(n-1)$-dimensional ellipsoidal surfaces; random coefficients transform discrete fixed combinations into continuous sampling *on* those surfaces, mitigating the discrete-cluster bias of the conventional MPF (Fig. 3) and yielding a smoother redistribution. By contrast, when $n > d+1$ (volumetric resampling), the induced density is continuous over a bounded region and *fills* previously unoccupied areas of the state space, providing effective regularization against degeneracy.

Pre-merging estimates outperform post-merging ones by $\approx$ 7–10% (Tables 4, 7). Because merging displaces particles from their observation-informed locations, it inevitably incurs some information loss at time t. This supports treating merging primarily as a diversity-regularization step for future times, while adopting the pre-merging ensemble mean as the estimate at time t.

https://doi.org/10.5194/egusphere-2026-4073
Preprint. Discussion started: 21 July 2026

Building on these observations, we adopted a likelihood–maximization criterion for selecting the merging dimension n (Section 8). This approach is used directly when ground truth is unavailable, as it relies on the pre-merging predictive log-likelihood, which is a strictly proper scoring rule theoretically grounded in Bayesian estimation. It is dimension-agnostic (applicable regardless of d), and operationally simple to implement within the RMPF pipeline. Empirically, it tracks RMSE well and provides a single, tunable objective for choosing n across different particle budgets and models, thereby removing a major practical obstacle to deploying RMPF in real-world settings.

9.2 Relation to Existing Approaches

Regularized Particle Filters (RPF) smooth the empirical measure via kernel density estimation (KDE) and then resample; performance hinges on bandwidth and scales poorly in high d (Musso et al., 2001). **Gaussian Sum Particle Filters (GSPF)** approximate the distribution with a weighted Gaussian mixture, that is, a set of parallel Gaussian filters, offering multimodality through Gaussian assumptions and component management (Kotecha and Djuric, 2003). **RMPF** achieves implicit kernel-like smoothing directly through merging with a compact-support polynomial kernel; smoothness is governed by n (not bandwidth). In practice, this yields favorable $O(N \times n \times d)$ cost and avoids per-step KDE or mixture maintenance.

The RPF/GSPF constructs a distribution followed by resampling, whereas RMPF performs direct resampling via merging under simplex–sphere constraints. This design preserves the PF as a special case when merging is disabled ($n = 1$), which explains why, in Lorenz96, $n \gtrsim d$ systematically improves RMSE while reducing the required N by $4\times$ to $8\times$ (Table 6).

10 Conclusions and Future Challenges

10.1 Research Overview and Main Achievements

This study proposed RMPF to solve two fundamental challenges of merging particle filter: the "lack of an established method for setting the merging coefficients" and "RMSE saturation with increasing particle numbers." RMPF adopts two approaches to address these limitations. The first approach employs random merging coefficients, which eliminates fixed coefficient bias through coefficient generation from spherical uniform distribution. The second approach utilizes pre-merging estimate calculation, which avoids the information loss from merging operations and maximally utilizes observation information.

In numerical experiments, RMPF demonstrated good performance across multiple dimensions. The method achieved particle number reduction effects, requiring only 1/4 to 1/8 the particle number of standard PF to achieve equivalent accuracy in both Lorenz63 and Lorenz96 models. RMPF successfully resolved the RMSE saturation problem that plagues the conventional MPF, maintaining stable performance improvement even with large particle numbers. The method confirmed high-dimensional applicability, demonstrating consistent effectiveness across systems ranging from 3 to 40 dimensions. Additionally, pre-merging estimates consistently outperformed post-merging estimates by 7-10% across all experiments.

https://doi.org/10.5194/egusphere-2026-4073
Preprint. Discussion started: 21 July 2026

10.2 Theoretical Contributions

Through probability density analysis of merged particles, we theoretically clarified that the relationship between merging dimension n and state space dimension d determines the distribution characteristics. When $n < r + 2$, the system exhibits edge concentration distribution with particles concentrated in the periphery. When $n = r + 2$, a uniform distribution emerges across the constraint region. When $n > r + 2$, governed by Eq. (24), the center of each merged-particle distribution moves closer to the ensemble mean as n increases. This theoretical prediction was verified by experiments, providing a solid foundation for merging dimension selection.

10.3 Practical Significance

A strong negative correlation was observed between log-likelihood and RMSE, which enabled us to establish a method for merging dimension using likelihood maximization, applicable to real applications where true values are unknown. This approach addressed the major technical obstacles in practical implementation of RMPF, allowing it to be deployed in real-world scenarios without ground truth information.

10.4 Future Challenges

Several important research directions remain to be explored. The extension to non-Gaussian observation models represents a significant challenge, requiring comprehensive analysis of RMPF performance, with observations exhibiting strong non-Gaussianity. Adaptive merging dimension control presents another crucial area for development, focusing on dynamic dimension adjustment for time-varying systems and sudden events. The verification of RMPF is essential in large-scale practical systems, including integration with atmospheric and ocean models and development of localization strategies for extremely high-dimensional applications. Finally, theoretical convergence analysis requires rigorous mathematical investigation of the convergence properties and rates in high-dimensional limits to strengthen the theoretical foundation of the method.

10.5 Closing Remarks

In summary, RMPF is an effective method that improves computational efficiency and estimation accuracy of data assimilation in high-dimensional nonlinear systems. Together with grounded merging dimension selection guidelines, practical applications in diverse fields are expected. The achievements of this research greatly enhance the practicality of particle filters and open the path for more complex system applications.

Code and data availability. The source code of the Randomized Merging Particle Filter (RMPF) and the scripts and synthetic data files required to reproduce all figures and tables in this manuscript are archived on Zenodo (Hiramoto et al., 2026) (https://doi.org/10.5281/zenodo.20924024) under the MIT license. All observations are synthetic and are generated from the Lorenz-63 and Lorenz-96 models within

https://doi.org/10.5194/egusphere-2026-4073
Preprint. Discussion started: 21 July 2026

the provided scripts; no external data are required. The record is currently released with restricted file access and will be made openly available upon publication. During the review process, the files have been made accessible to the editor and referees.

Appendix A: Preservation of the First Two Moments

A1 Mean

Even if each post–merging particle uses its own coefficients $\{\alpha_j^i\}_{j=1}^n$, as long as $\sum_{j=1}^n \alpha_j^i = 1$ holds for all i, the ensemble mean is preserved. The mean of the post–merging empirical distribution is

$$\int \mathbf{x}_t \frac{1}{N}\sum_{i=1}^{N} \delta\Big(\mathbf{x}_t - \mathbf{x}_t^{(i)}\Big)\, d\mathbf{x}_t = \frac{1}{N}\sum_{i=1}^{N} \mathbf{x}_t^{(i)} \tag{A1}$$

$$= \frac{1}{N}\sum_{i=1}^{N}\sum_{j=1}^{n} \alpha_j^i\, \hat{\mathbf{x}}_t^{j,i} \tag{A2}$$

$$= \sum_{j=1}^{n}\left[\frac{1}{N}\sum_{i=1}^{N} \alpha_j^i\, \hat{\mathbf{x}}_t^{j,i}\right]. \tag{A3}$$

Here $\{\hat{\mathbf{x}}_t^{j,1}, \ldots, \hat{\mathbf{x}}_t^{j,N}\}$ are obtained by (weighted) resampling. As $N \to \infty$,

$$\frac{1}{N}\sum_{i=1}^{N} \hat{\mathbf{x}}_t^{j,i} \;\approx\; \int \mathbf{x}_t\, p(\mathbf{x}_t \mid \mathbf{y}_{1:t})\, d\mathbf{x}_t \;=\; \boldsymbol{\mu}_t. \tag{A4}$$

Since the n resampled sets are independent of j, their means converge to the same limit. Writing $\bar{\alpha}_j := \frac{1}{N}\sum_{i=1}^{N} \alpha_j^i$, we obtain, for large N,

$$\frac{1}{N}\sum_{i=1}^{N}\sum_{j=1}^{n} \alpha_j^i\, \hat{\mathbf{x}}_t^{j,i} \approx \sum_{j=1}^{n} \bar{\alpha}_j \int \mathbf{x}_t\, p(\mathbf{x}_t \mid \mathbf{y}_{1:t})\, d\mathbf{x}_t \tag{A5}$$

$$= \Big(\sum_{j=1}^{n} \bar{\alpha}_j\Big)\, \boldsymbol{\mu}_t \;=\; \boldsymbol{\mu}_t, \tag{A6}$$

because $\sum_{j=1}^n \bar{\alpha}_j = 1$. Thus, the post–merging ensemble mean asymptotically equals the filter mean $\boldsymbol{\mu}_t$.

A2 Covariance

Next, preservation of the covariance matrix. The empirical covariance of the post–merging ensemble is

$$\int (\mathbf{x}_t - \boldsymbol{\mu}_t)(\mathbf{x}_t - \boldsymbol{\mu}_t)^\top \frac{1}{N}\sum_{i=1}^{N} \delta(\mathbf{x}_t - \mathbf{x}_t^{(i)})\, d\mathbf{x}_t$$

$$= \frac{1}{N}\sum_{i=1}^{N} (\mathbf{x}_t^{(i)} - \boldsymbol{\mu}_t)(\mathbf{x}_t^{(i)} - \boldsymbol{\mu}_t)^\top. \tag{A7}$$

https://doi.org/10.5194/egusphere-2026-4073
Preprint. Discussion started: 21 July 2026

Substituting $\mathbf{x}_t^{(i)} = \sum_{j=1}^n \alpha_j^i \hat{\mathbf{x}}_t^{j,i}$, we obtain

$$\frac{1}{N}\sum_{i=1}^{N}\Big[\sum_{j_1=1}^{n}\alpha_{j_1}^{i}\big(\hat{\mathbf{x}}_t^{j_1,i}-\boldsymbol{\mu}_t\big)\Big] \times\Big[\sum_{j_2=1}^{n}\alpha_{j_2}^{i}\big(\hat{\mathbf{x}}_t^{j_2,i}-\boldsymbol{\mu}_t\big)\Big]^{\top}. \tag{A8}$$

For $j_1 \neq j_2$, the samples $\hat{\mathbf{x}}_t^{j_1,i}$ and $\hat{\mathbf{x}}_t^{j_2,i}$ are drawn independently; hence, as $N \to \infty$,

$$\frac{1}{N}\sum_{i=1}^{N}\big(\hat{\mathbf{x}}_t^{j_1,i}-\boldsymbol{\mu}_t\big)\big(\hat{\mathbf{x}}_t^{j_2,i}-\boldsymbol{\mu}_t\big)^{\top} \approx \mathbf{0}. \tag{A9}$$

Thus off–diagonal ($j_1 \neq j_2$) contributions vanish asymptotically, and

$$\frac{1}{N}\sum_{i=1}^{N}\sum_{j=1}^{n}(\alpha_j^i)^2\big(\hat{\mathbf{x}}_t^{j,i}-\boldsymbol{\mu}_t\big)\big(\hat{\mathbf{x}}_t^{j,i}-\boldsymbol{\mu}_t\big)^{\top}. \tag{A10}$$

If, in addition, $\sum_{j=1}^n(\alpha_j^i)^2 = 1$ holds for all i, then with $\bar{\beta}_j := \frac{1}{N}\sum_{i=1}^N(\alpha_j^i)^2$ we have $\sum_{j=1}^n \bar{\beta}_j = 1$, as $N \to \infty$,

$$\begin{aligned}&\sum_{j=1}^{n}\frac{1}{N}\sum_{i=1}^{N}(\alpha_j^i)^2\big(\hat{\mathbf{x}}_t^{j,i}-\boldsymbol{\mu}_t\big)\big(\hat{\mathbf{x}}_t^{j,i}-\boldsymbol{\mu}_t\big)^{\top}\\ &\approx\sum_{j=1}^{n}\bar{\beta}_j\int(\mathbf{x}_t-\boldsymbol{\mu}_t)(\mathbf{x}_t-\boldsymbol{\mu}_t)^{\top}p(\mathbf{x}_t\mid\mathbf{y}_{1:t})\,d\mathbf{x}_t\\ &=\Big(\sum_{j=1}^{n}\bar{\beta}_j\Big)\boldsymbol{\Sigma}_t \;=\; \boldsymbol{\Sigma}_t.\end{aligned} \tag{A11}$$

Hence, under the constraints $\sum_j \alpha_j^i = 1$ and $\sum_j (\alpha_j^i)^2 = 1$ for all i, the post–merging ensemble asymptotically preserves both the mean and covariance $(\boldsymbol{\mu}_t, \boldsymbol{\Sigma}_t)$ of the filter distribution.

Appendix B: Derivation of the Normalization Constant

To derive the normalization constant $C_{n,r}$, we integrate the induced (unnormalized) density over the feasible region. When $\mathrm{rank}(A) = r$, the null space has dimension $m = n - r$ and any solution can be written as $\boldsymbol{\alpha} = \boldsymbol{\alpha}^* + B\boldsymbol{z}$, where $B \in \mathbb{R}^{n\times m}$ is an orthonormal basis of $\ker(A)$. The unit–sphere constraint $\|\boldsymbol{\alpha}\|^2 = 1$ reduces to

$$\begin{aligned}\|\boldsymbol{z}\|^2 &= R^2(\mathbf{x}_{\text{merged}})\\ &:= \frac{n-1}{n} - (\mathbf{x}_{\text{merged}}-\bar{\mathbf{x}})^{\top}(XPX^{\top})^{+}(\mathbf{x}_{\text{merged}}-\bar{\mathbf{x}}),\end{aligned}$$

so $\boldsymbol{z}$ lies on the $(m-1)$–sphere of radius R whenever $R^2 \geq 0$.

https://doi.org/10.5194/egusphere-2026-4073
Preprint. Discussion started: 21 July 2026

B0.1 Step 1: Delta constraint for the radius.

For fixed X, the induced density at $\mathbf{x}_{\text{merged}}$ is (up to a constant)

$$p(\mathbf{x}_{\text{merged}} \mid X) \propto \int_{\mathbb{R}^m} \delta\big(\mathbf{x}_{\text{merged}} - X\boldsymbol{\alpha}^* - XB\boldsymbol{z}\big) \times \delta\big(\|\boldsymbol{z}\|^2 - R^2\big)\, d\boldsymbol{z}. \tag{B1}$$

In spherical coordinates, $r = \|\boldsymbol{z}\|$ and $\delta(r^2 - R^2) = \delta(r - R)/(2R)$ for $r \geq 0$; integration yields

$$\int_{\mathbb{R}^m} \delta(\|\boldsymbol{z}\|^2 - R^2)\, d\boldsymbol{z} = \frac{1}{2R} \int_{S^{m-1}(R)} dS(\boldsymbol{z}), \qquad S_{m-1}(R) = \frac{2\pi^{m/2}}{\Gamma(m/2)} R^{m-1}. \tag{B2}$$

B0.2 Step 2: Linear–map Jacobian.

Under $\boldsymbol{z} \mapsto \mathbf{x}_{\text{merged}} = X\boldsymbol{\alpha}^* + XB\boldsymbol{z}$, the $(m-1)$–dimensional surface measure is transformed with Jacobian $\sqrt{\det{}'((XB)(XB)^\top)}$ on the image subspace. Writing $P = I_n - \frac{1}{n}\mathbf{1}\mathbf{1}^\top$ and $\Sigma := XPX^\top$, this contributes the factor $\big|\det{}'(\Sigma)\big|^{-1/2}$.

B0.3 Step 3: Volumetric factor.

Combining (B2) with $S_{m-1}(R) \propto R^{m-1}$ gives the factor $R^{m-1} \cdot (1/2R) \propto (R^2)^{(m-2)/2}$. Therefore, with $m = n - r$,

$$p(\mathbf{x}_{\text{merged}} \mid X) \propto \big|\det{}'(XPX^\top)\big|^{-1/2} \big[R^2(\mathbf{x}_{\text{merged}})\big]_+^{\frac{m-2}{2}}, \qquad [u]_+ := \max\{u, 0\}. \tag{B3}$$

B0.4 Normalization.

To normalize (B3), we integrate over the ellipsoidal region $R^2 > 0$. Let L satisfy $(XPX^\top)^+ = L^\top L$ and substituting $\mathbf{t} = L(\mathbf{x}_{\text{merged}} - \bar{\mathbf{x}})$, we obtain

$$\int_{\|\mathbf{t}\| \leq \sqrt{a}} (a - \|\mathbf{t}\|^2)^\beta\, d\mathbf{t},$$

$$a = \frac{n-1}{n}, \quad \beta = \frac{n-r-2}{2}, \quad k = \operatorname{rank}(XPX^\top) = r - 1,$$

evaluates to $a^{\beta + k/2}\, \dfrac{\pi^{k/2}\Gamma(\beta+1)}{\Gamma(\beta+1+k/2)}$, yielding

$$C_{n,r} = \frac{\Gamma\left(\frac{n-1}{2}\right)}{\pi^{\frac{r-1}{2}}\, \Gamma\left(\frac{n-r}{2}\right)} \left(\frac{n}{n-1}\right)^{\frac{n-3}{2}}, \tag{B4}$$

valid for $n > r + 1$ $(\beta > -1)$.

This constant captures how the merging dimension n and effective dimension r of the augmented system shape the induced density.

https://doi.org/10.5194/egusphere-2026-4073
Preprint. Discussion started: 21 July 2026

Author contributions. NH designed the method, implemented the experiments, and wrote the manuscript. GU and DM supervised the study and revised the manuscript. All authors discussed the results and approved the final version.

Competing interests. The authors declare that they have no conflict of interest.

Acknowledgements. The numerical experiments in this study were performed using the Supercomputer System for Data Assimilation at the Institute of Statistical Mathematics, Research Organization of Information and Systems.

Financial support. This research received no external funding.

https://doi.org/10.5194/egusphere-2026-4073
Preprint. Discussion started: 21 July 2026

References

Bengtsson, T., Bickel, P., and Li, B.: Curse of dimensionality revisited: Collapse of the particle filter in very large scale systems, in: Probability and Statistics: Essays in Honor of David A. Freedman, edited by Nolan, D. and Speed, T., pp. 316–334, Institute of Mathematical Statistics, 2008.

Chen, Z. and Haykin, S.: On different facets of regularization theory, Neural Computation, 14, 2791–2846, 2002.

Cooper, M. and Perez, T.: Dual-particle-filtering for recursive estimation of agricultural-machinery dynamics, IFAC-PapersOnLine, 51, 658–663, 2018.

Darányi, A. and Abonyi, J.: Fault diagnostics based on the analysis of probability distributions estimated using a particle filter, Sensors, 24, 719, 2024.

Daum, F. and Huang, J.: Particle degeneracy: Root cause and solution, in: Proceedings of SPIE, vol. 8050, p. 7167, https://doi.org/10.1117/12.877167, 2011.

Davis, R. A., Lii, K.-S., and Politis, D. N.: Remarks on some nonparametric estimates of a density function, in: Selected Works of Murray Rosenblatt, pp. 95–100, Springer, 2011.

Douc, R., Moulines, E., and Rydén, T.: Asymptotic properties of the maximum likelihood estimator in autoregressive models with Markov regime, 2004.

Fan, Z.: MLE under model misspecification, Lecture 16, STATS 200: Introduction to Statistical Inference, Stanford University, https://web.stanford.edu/class/archive/stats/stats200/stats200.1172/Lecture16.pdf, autumn 2016, 2016.

Gneiting, T. and Raftery, A. E.: Strictly proper scoring rules, prediction, and estimation, Journal of the American statistical Association, 102, 359–378, 2007.

Gordon, N., Salmond, D., and Smith, A. F. M.: Novel approach to nonlinear and non-Gaussian Bayesian state estimation, IEE Proceedings F - Radar and Signal Processing, 140, 107–113, https://doi.org/10.1049/ip-f-2.1993.0015, 1993.

Gustafsson, F.: Particle filter theory and practice with positioning applications, IEEE Aerospace and Electronic Systems Magazine, 25, 53–82, 2010.

Hiramoto, N., Ueno, G., and Murakami, D.: Replication package of Randomized Merging Particle Filter, Zenodo, https://doi.org/10.5281/zenodo.20924024, version v2, MIT license [code], 2026.

Hoteit, I., Luo, X., and Pham, D.-T.: Particle Kalman filtering: A nonlinear Bayesian framework for ensemble Kalman filters, Monthly weather review, 140, 528–542, 2012.

Ito, T., Matsuda, T., Hayashino, Y., and Sakuraba, H.: Seepage analysis model based on field measurement data for estimation of posterior parameter distribution using merging particle filter, Soils and Foundations, 64, 101 442, https://doi.org/10.1016/j.sandf.2024.101442, 2024.

Kenyeres, É. and Abonyi, J.: Goal-Oriented Tuning of Particle Filters for the Fault Diagnostics of Process Systems, Processes, 11, 823, 2023.

Kitagawa, G.: Monte Carlo filter and smoother for non-Gaussian nonlinear state space models, Journal of Computational and Graphical Statistics, 5, 1–25, https://doi.org/10.1080/10618600.1996.10474692, 1996.

Kotecha, J. H. and Djuric, P. M.: Gaussian sum particle filtering, IEEE Transactions on Signal Processing, 51, 2602–2612, 2003.

Kummert, J., Schulz, A., Redick, T., et al.: Efficient reject options for particle filter object tracking in medical applications, Sensors, 21, 2114, 2021.

https://doi.org/10.5194/egusphere-2026-4073
Preprint. Discussion started: 21 July 2026

Li, T., Sun, S., Sattar, T. P., and Corchado, J. M.: Fight sample degeneracy and impoverishment in particle filters: A review of intelligent approaches, Expert Systems with Applications, 41, 3944–3954, 2014.

Liu, J. and West, M.: Combined parameter and state estimation in simulation-based filtering, in: Sequential Monte Carlo methods in practice, pp. 197–223, Springer, 2001.

Lorenz, E. N.: Deterministic non-periodic flows, Journal of the Atmospheric Sciences, 20, 130–141, 1963.

Lorenz, E. N.: Predictability: A problem partly solved, in: Proc. Seminar on predictability, vol. 1, pp. 1–18, Reading, 1996.

Maclean, J. and Spiller, E. T.: A surrogate-based approach to nonlinear, non-Gaussian joint state-parameter data assimilation, arXiv preprint arXiv:2012.04793, 2020.

Maclean, J., Santitissadeekorn, N., and Jones, C. K.: A coherent structure approach for parameter estimation in Lagrangian Data Assimilation, Physica D: Nonlinear Phenomena, 360, 36–45, 2017.

Muller, M. E.: A note on a method for generating points uniformly on N-dimensional spheres, Communications of the ACM, 2, 19, 1959.

Musso, C., Oudjane, N., and Le Gland, F.: Improving regularized particle filters, in: Sequential Monte Carlo Methods in Practice, edited by Doucet, A., de Freitas, N., and Gordon, N., pp. 247–271, Springer-Verlag, 2001.

Nakano, S. and Higuchi, T.: Estimation of a Long-Term Variation of a Magnetic-Storm Index Using the Merging Particle Filter, IEICE Transactions on Information and Systems, E92-D, 1382–1392, https://doi.org/10.1587/transinf.E92.D.1382, 2009.

Nakano, S. and Higuchi, T.: Non-storm irregular variation of the Dst index, Annales Geophysicae, 30, 153–163, https://doi.org/10.5194/angeo-30-153-2012, 2012.

Nakano, S., Ueno, G., and Higuchi, T.: Merging particle filter for sequential data assimilation, Nonlinear Processes in Geophysics, 14, 395–408, https://doi.org/10.5194/npg-14-395-2007, 2007.

Nakano, S., Ueno, G., Nakamura, K., and Higuchi, T.: Merging Particle Filter and Its Characteristics, 2008.

Nomura, Y., Matsudaira, I., and IDE, K.: Structural Identification Based on AR Model For Earthquake Response and Merging Particle Filter, Journal of the Society of Materials Science, Japan, 68, 242–249, 2019.

Oudjane, N.: Stabilité et approximations particulaires en filtrage non linéaire application au pistage, Ph.D. thesis, Rennes 1, 2000.

Parzen, E.: On estimation of a probability density function and mode, The annals of mathematical statistics, 33, 1065–1076, 1962.

Pitt, M. K. and Shephard, N.: Filtering via simulation: Auxiliary particle filters, Journal of the American statistical association, 94, 590–599, 1999.

Poterjoy, J.: A localized particle filter for high-dimensional nonlinear systems, Monthly Weather Review, 144, 59–76, 2016.

Rossi, V.: Filtrage non linéaire par noyaux de convolution: application à un procédé de dépollution biologique, Ph.D. thesis, Montpellier, ENSA, 2004.

Shen, Z., Tang, Y., and Li, X.: A new formulation of vector weights in localized particle filters, Quarterly Journal of the Royal Meteorological Society, 143, 3269–3278, 2017.

Slivinski, L. and Snyder, C.: Exploring practical estimates of the ensemble size necessary for particle filters, Monthly Weather Review, 144, 861–875, https://doi.org/10.1175/MWR-D-14-00303.1, 2016.

Snyder, C., Bengtsson, T., Bickel, P., and Anderson, J.: Obstacles to High-Dimensional Particle Filtering, Monthly Weather Review, 136, 4629–4640, https://doi.org/10.1175/2008mwr2529.1, 2008.

Van Leeuwen, P. J.: Nonlinear data assimilation in geosciences: an extremely efficient particle filter, Quarterly Journal of the Royal Meteorological Society, 136, 1991–1999, 2010.

https://doi.org/10.5194/egusphere-2026-4073
Preprint. Discussion started: 21 July 2026

Van Leeuwen, P. J., Künsch, H. R., Nerger, L., Potthast, R., and Reich, S.: Particle filters for high-dimensional geoscience applications: A review, Quarterly Journal of the Royal Meteorological Society, 145, 2335–2365, 2019.

Vetra-Carvalho, S. et al.: State-of-the-art stochastic data assimilation methods for high-dimensional non-Gaussian problems, Tellus A: Dynamic Meteorology and Oceanography, 70, 1–43, https://doi.org/10.1080/16000870.2018.1445364, 2018.